Available online at www.sciencedirect.com
ScienceDirect
Journal of Computational Physics 227 (2008) 3212–3243
JOURNAL OF COMPUTATIONAL PHYSICS
www.elsevier.com/locate/jcp

# Exact solution of the Riemann problem for the shallow water equations with discontinuous bottom geometry

R. Bernetti [a,*], V.A. Titarev [b], E.F. Toro [c]

[a] *Politechnic Univeristy of Marche, Department of Mechanics, Ancona, Italy*
[b] *School of Engineering, Cranfield University, Bedfordshire MK43 0AL, United Kingdom*
[c] *Laboratory of Applied Mathematics, Department of Civil and Environmental Engineering, University of Trento, Trento, Italy*

Received 26 July 2007; received in revised form 20 November 2007; accepted 26 November 2007
Available online 8 December 2007

**Abstract**

In this paper we present the exact solution of the Riemann problem for the non-linear shallow water equations with a step-like bottom. The solution has been obtained by solving an enlarged system that includes an additional equation for the bottom geometry and then using the principles of conservation of mass and momentum across the step. The resulting solution is unique and satisfies the principle of dissipation of energy across the shock wave. We provide examples of possible wave patterns. Numerical solution of a first-order dissipative scheme as well as an implementation of our Riemann solver in the second-order upwind method are compared with the proposed exact Riemann problem solution. A practical implementation of the proposed exact Riemann solver in the framework of a second-order upwind TVD method is also illustrated.


*Keywords:* Shallow water equations; Discontinuous bottom geometry; Exact Riemann solver; WAF method

## 1. Introduction

The shallow water equations represent a popular mathematical model for free-surface flows arising in shores, rivers and many other physical situations [15]. Due to the non-linearity of the equations as well as the complexity of the geometries encountered in real-life applications much effort has been made in recent years to develop numerical methods to solve the equations approximately. In particular, Godunov-type methods [8] have proven popular due to their ability to treat discontinuities arising in the solution. For a review of modern finite-volume methods as applied to the shallow water equations see [18], for example. However, in spite of significant overall progress made in the field, serious problems still remain in dealing with geometric source terms arising in the shallow water equations in the case of non-uniform bottom geometry. Conventional techniques for treating the source terms produce erroneous results, and special effort is required to avoid

* Corresponding author.
*E-mail address:* roberto.bernetti@poste.it (R. Bernetti).

0021-9991/$ - see front matter © 2007 Elsevier Inc. All rights reserved.
doi:10.1016/j.jcp.2007.11.033

numerical artifacts when the bottom distribution varies rapidly. Similar problems arise in other hyperbolic systems with geometric source terms.

A popular approach to the construction of Godunov-type methods for hyperbolic systems with geometric source terms is to use the so-called upwind discretization of the source, first introduced by Roe in 1986 [14]. See also [7,12,19] and references therein. A particular variety of these schemes, the so called well-balanced schemes, the source terms are approximated so as to ensure that in the steady-state the flux gradient and the source terms are balanced, at least approximately. Another approach to the problem is to add an additional equation to the system describing the bottom behaviour in time and then try to construct a Riemann solver for the extended system, see e.g. [6]. The idea is that the scheme using such a Riemann solver will not be prone to the problems encountered in conventional advection methods. We also mention the so-called surface-reconstruction method [10] for constructing well-balanced schemes, in which an appropriate choice of variables is chosen to reformulate the equations.

In this work, we present an exact solution of the Riemann problem for the shallow water equations with a discontinuous bottom geometry. The method uses two main assumptions. Firstly, conservation of mass and momentum are used to derive the Rankine–Hugoniot conditions across the bottom step. Secondly, in order to exclude the multiplicity of solutions, we impose that the entropy condition be fulfilled; that is, total energy dissipates across the stationary shock wave at the step and transition from subcritical to supercritical flow across an upward step is excluded. We then show that the resulting self-similar solution is unique and can be constructed in a conventional way by solving an algebraic system of two equations for the so-called *star values* for depth and velocity.

To assess our new solution we present a number of numerical examples. First, we compare our exact solution with numerical solutions of a first-order centred scheme. Good agreement is observed. Next, we illustrate a practical use of the developed exact Riemann solver by incorporating it into the Weighted Average Flux (WAF) method [16,17,4,3], which is a second-order Godunov-type TVD scheme. A detailed evaluation of the resulting scheme is the subject of current investigations by the authors, of which some encouraging preliminary results are shown here.

There are currently in the literature some published works that are related to the present paper; see for example [1,11,5]. In [5] the authors analyze the particular case of zero initial velocity on the side of the interface with the lower depth and show that under the energy conservation condition the stated Riemann problem is unsolvable. To overcome this they consider two different options. In the first option an heuristic parameter is introduced that defines the part of the total flow energy that is lost in the transition over the drop. In the second option the continuity of the flow rate is imposed over the drop. This option is similar to ours.

The rest of the paper is organized as follows. In Section 2 we analyze the structure of the system of equations of interest. In Section 3 the solution of the Riemann problem with a discontinuous piece-wise constant bottom geometry is presented. Examples of possible solution patterns are given in Section 4 for a number of wave patterns. Comparison of the exact solution and the numerical solution of a first-order dissipative scheme as well as an implementation of our Riemann solver in the second-order upwind method are shown in Section 5. Conclusions are drawn in Section 6.

## 2. Shallow water equations with a source term

We consider the augmented one-dimensional system of shallow water equations (SWE) with a discontinuous bottom in the following form:

$$\begin{aligned}
&\frac{\partial}{\partial t}\phi + \frac{\partial}{\partial x}(\phi u) = 0\\
&\frac{\partial}{\partial t}(\phi u) + \frac{\partial}{\partial x}(\phi u^2 + \frac{1}{2}\phi^2) = g\phi\frac{\partial}{\partial x}h\\
&\frac{\partial}{\partial t}(\phi v) + \frac{\partial}{\partial x}(\phi uv) = 0\\
&\frac{\partial}{\partial t}h = 0
\end{aligned} \tag{1}$$

Here $\eta$ is the free-surface elevation, $h$ is the bottom depth with respect to the $z$ plane, $u$ and $v$ are the components of velocity in $x$ and $y$ directions respectively, $g$ is the acceleration due to gravity, $d = h + \eta$ is the total depth, $c = \sqrt{gd}$ is the celerity and $\phi = c^2$. See Fig. 1 for a graphical explanation of the variables. An additional, fourth equation for the bottom has been added to the system of equations in a manner similar to that used in [11] for the equations of gas dynamics. In this section we first study the eigenstructure of the resulting modified system of equations and derive Rankine–Hugoniot conditions by applying the laws of mass and momentum conservation to a finite mass of fluid across the bottom discontinuity.

### 2.1. Eigenvalues and eigenvectors for the modified SWE

To carry out the eigenstructure analysis we rewrite (1) in quasilinear following form:

$$\frac{\partial}{\partial t}U + A\frac{\partial}{\partial x}U = 0$$

where the vector of conservative variables $U$ and the matrix $A$ are given by:

$$U = \begin{bmatrix} \phi \\ \phi u \\ \phi v \\ h \end{bmatrix} = \begin{bmatrix} u_1 \\ u_2 \\ u_3 \\ u_4 \end{bmatrix}, \quad A = \begin{bmatrix} 0 & 1 & 0 & 0 \\ -(u_2/u_1)^2 + u_1 & 2u_2/u_1 & 0 & gu_1 \\ -u_2u_3/u_1^2 & u_3/u_1 & u_2/u_1 & 0 \\ 0 & 0 & 0 & 0 \end{bmatrix}$$

The matrix $A$ has the following four real eigenvalues:

$$\lambda_1 = u - \sqrt{\phi}, \quad \lambda_2 = 0, \quad \lambda_3 = u, \quad \lambda_4 = u + \sqrt{\phi}$$

The set of corresponding left eigenvectors is given by:

$$\mathbf{L} = \begin{pmatrix} l_1 \\ l_2 \\ l_3 \\ l_4 \end{pmatrix} = \begin{pmatrix} (u_1^3 - u_2^2)/u_1^2 & (u_1u_2 - u_1^{5/2})/u_1^2 & 0 & gu_1 \\ 0 & 0 & 0 & 1 \\ -u_2/u_1 & 0 & 1 & 0 \\ (u_1^3 - u_2^2)/u_1^2 & (u_1u_2 + u_1^{5/2})/u_1^2 & 0 & gu_1 \end{pmatrix}$$

A standard procedure shows that the second and third eigenvectors correspond to the following Riemann invariants:

$$h = \text{const}, \quad v = \text{const}$$

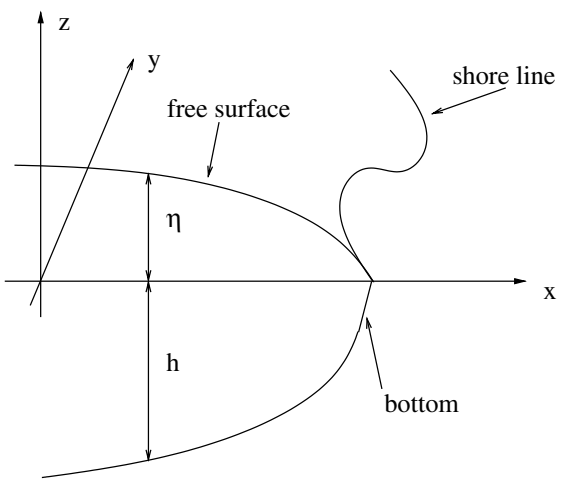


Fig. 1. Reference frame and physical variable.

The equations along characteristics for the first and fourth eigenvectors are similar and we therefore analyze only the first one. For the first characteristic curve we have:

$$\frac{(u_1^{3/2}+u_2)}{u_1^2}\mathrm{d}u_1+\frac{\mathrm{d}u_2}{u_1}+gu_1(u_1^{3/2}-u_2)^{-1}\mathrm{dh}=0 \tag{2}$$

As one may expect, the equation for the Riemann invariant depends on the bottom variation. For the rest of the paper we assume that $h(x)$ is a piecewise constant function. Therefore, where $h(x)$ is continuous (away from the discontinuity) we have $\mathrm{dh}=0$, and the corresponding first Riemann invariant coincides with the conventional one and is given by:

$$u-2\sqrt{\phi}=\text{const} \tag{3}$$

Similarly, the fourth invariant is given by:

$$u+2\sqrt{\phi}=\text{const} \tag{4}$$

Therefore, we have established that if the bottom variation is piecewise constant then the characteristic lines and Riemann invariants of (1) in the regions where $h(x)$ is constant coincide with those of the conventional shallow water equations without the geometric source term. The same conclusion was drawn in [11] for a system of gas dynamical equations with a source term.

### 2.2. Rankine–Hugoniot condition for a discontinuous bottom

Assume that the initial left and right states are connected by a single discontinuity. We consider a flow region made up of water lying between two vertical planes $\pi_L$ and $\pi_R$, as depicted in Fig. 2. Let us again denote the quantities on the left side of the discontinuity by the index $L$ and those on the right by $R$. That is $U_L$ is the left state vector and $U_R$ is the right one. Without loss of generality we assume that $h_L > h_R$, in fact, due to the symmetry property of the flow, the solution for the case $h_L < h_R$ can be obtained exchanging the $L$ and $R$ subcripts. Referring to Fig. 2 $x_L(t)$, $x_R(t)$ and $s(t)$ are respectively the position of the plane $\pi_L$, of the plane $\pi_R$ and of the position of the discontinuity of the water surface at time $t$.

For the following mathematical development we assume, as common in Shallow Water Theory, the following [15]:

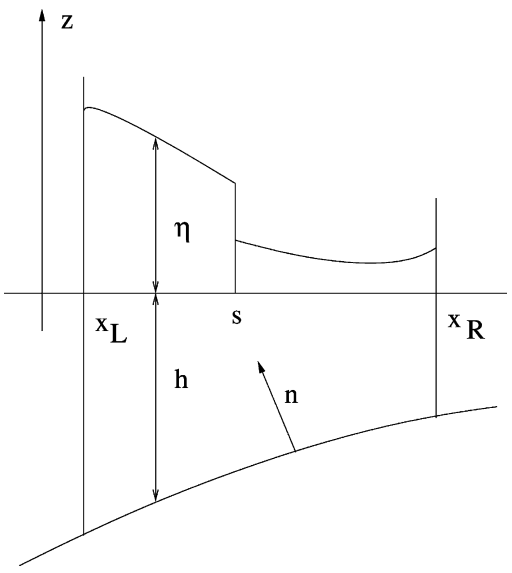


Fig. 2. Sketch of the Rankine–Hugoniot conditions.

**Definition 2.1.** Particles in a vertical plane at any instant always remain in a vertical plane, i.e. the streamwise velocity is uniform over the vertical.

**Definition 2.2.** The planes $\pi_L$ and $\pi_R$ are chosen such that they always contain the same particles hence the integration volume are moving with the fluid.

With the previous assumptions we have chosen a material reference frame to describe the motion of the fluid. Application of the conservation principles in this frame reduce to the condition that the material derivative of the mass be equal to zero while that of $x$-component of the first-order momentum be equal to the sum of surface and volume forces acting on the fluid volume [15]:

$$\frac{\mathrm{d}}{\mathrm{d}t}\int_{x_L(t)}^{x_R(t)}\int_{-h}^{\eta}\rho\,\mathrm{d}z\,\mathrm{d}x = 0$$
$$\frac{\mathrm{d}}{\mathrm{d}t}\int_{x_L(t)}^{x_R(t)}\int_{-h}^{\eta}\rho u\,\mathrm{d}z\,\mathrm{d}x = \int_{-h(x_L)}^{\eta(x_L)} p\,\mathrm{d}z + \int_{x_L(t)}^{x_R(t)} pn_x\,\mathrm{d}x - \int_{-h(x_R)}^{\eta(x_R)} p\,\mathrm{d}z$$

where $\rho$ is the fluid density, $p$ is the pressure and $n_x$ is the component of the normal to the bottom surface in the $x$ direction. The previous equation continue to be valid if the shock velocity is $\dot{s} = 0$. We now make the assumption of hydrostatic pressure distribution, that is

$$p(x,z) = \rho g(\eta(x) - z)$$

After integration in the $z$-direction the above system can be rewritten as:

$$\begin{aligned}
&\frac{\mathrm{d}}{\mathrm{d}t}\int_{x_L(t)}^{x_R(t)}\rho(\eta(x)+h(x))\mathrm{d}x = 0\\
&\frac{\mathrm{d}}{\mathrm{d}t}\int_{x_L(t)}^{x_R(t)}\rho(\eta(x)+h(x))u\,\mathrm{d}x = +\frac{1}{2}\rho g(\eta(x_L)+h(x_L))^2 + \int_{x_L(t)}^{x_R(t)} pn_x\,\mathrm{d}x - \frac{1}{2}\rho g(\eta(x_R)+h(x_R))^2
\end{aligned} \tag{5}$$

The integrals in $\mathrm{d}x$ are in the form:

$$I = \int_{x_L(t)}^{x_R(t)} \Psi(x,t)\mathrm{d}x \tag{6}$$

where $\Psi(x,t)$ is discontinuous at $x = s(t)$, this results in:

$$I = \int_{x_L(t)}^{s(t)} \Psi(x,t)\mathrm{d}x + \int_{s(t)}^{x_R(t)} \Psi(x,t)\mathrm{d}x \tag{7}$$

Differentiation under the integral sign gets:

$$\frac{\mathrm{d}I}{\mathrm{d}t} = \int_{x_L(t)}^{s(t)} \frac{\mathrm{d}\Psi(x,t)}{\mathrm{d}t}\,\mathrm{d}x + \int_{s(t)}^{x_R(t)} \frac{\mathrm{d}\Psi(x,t)}{\mathrm{d}t}\,\mathrm{d}x + \Psi(s^-,t)\dot{s}(t) - \Psi(x_L(t),t)u_L - \Psi(s^+,t)\dot{s}(t) + \Psi(x_R(t),t)u_R \tag{8}$$

where $u_L$ and $u_R$ are respectively the velocity of left and right fluid plane, $\Psi(s^-,t)$ and $\Psi(s^+,t)$ the limit values of $\Psi(x,t)$ to the left and to the right of the shock at $s$.

Dealing with discontinuous bottom we have to consider a more general configuration as in Fig. 3. In this case the bottom pressure action can be analyzed as follows:

$$\int_{x_L}^{x_R} pn_x\,\mathrm{d}x = \int_{x_L(t)}^{s(t)} pn_x\,\mathrm{d}x + \int_{s(t)}^{x_R(t)} pn_x\,\mathrm{d}x - \int_{-h(s^-)}^{-h(s^+)} p\,\mathrm{d}z \tag{9}$$

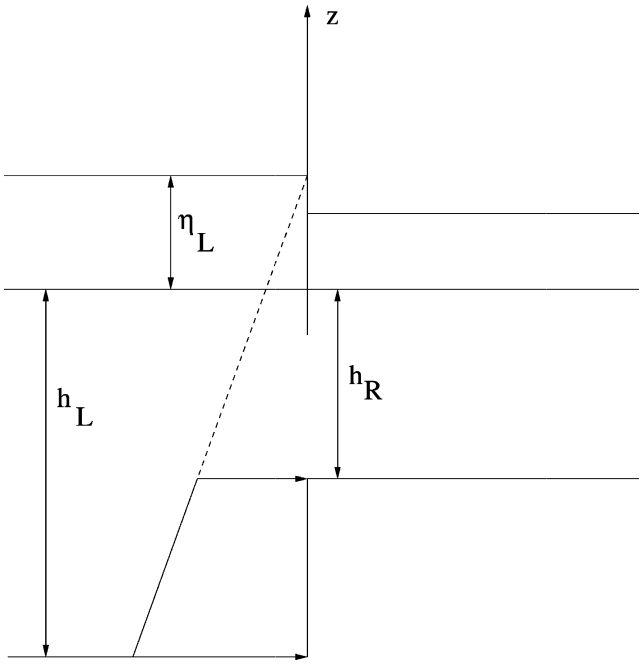


Fig. 3. Action exerted by the fluid on the step surface.

Now we have to consider the limit case when $x_L \to s$ and $x_R \to s$ which leads for mass and momentum integrals to:

$$\begin{aligned} &\lim_{x_L \to s} \int_{x_L(t)}^{s(t)} \frac{d\Psi(x,t)}{dt}\, dx = 0 \\ &\lim_{x_R \to s} \int_{s(t)}^{x_R(t)} \frac{d\Psi(x,t)}{dt}\, dx = 0 \end{aligned} \tag{10}$$

and for the pressure:

$$\begin{aligned} &\lim_{x_L \to s} \int_{x_L(t)}^{s(t)} pn_x\, dx = 0 \\ &\lim_{x_R \to s} \int_{s(t)}^{x_R(t)} pn_x\, dx = 0 \end{aligned} \tag{11}$$

Using results of Eqs. (8)–(11) into (5) and defining $d = h + \eta$:

$$\begin{aligned} &(\rho d_L - \rho d_R)\dot{s} - \rho d_L \cdot u_L + \rho d_R \cdot u_R = 0 \\ &(\rho d_L u_L - \rho d_R u_R)\dot{s} - \rho d_L \cdot u_L^2 + \rho d_R \cdot u_R^2 = +\frac{1}{2}\rho g d_L^2 - \frac{1}{2}\rho g d_R^2 - \frac{1}{2}\rho g[d_L + (\eta_L + h_R)](h_L - h_R) \end{aligned} \tag{12}$$

Defining "[ ]" as the jump across the discontinuity, e.g. $[\rho d] = \rho d_R - \rho d_L$, etc., we obtain the following relations:

$$\begin{aligned} &-\dot{s}[\rho d] + [\rho d u] = 0 \\ &-\dot{s}[\rho d u] + [\rho d u^2] = -[\frac{1}{2}\rho g d^2] + H \end{aligned} \tag{13}$$

The term $H$ is responsible for the bottom variation and represents the force exerted by the fluid on the step surface (with minus sign), see Fig. 3:

$$H = -\frac{1}{2}\rho g[d_L + (\eta_L + h_R)](h_L - h_R) \tag{14}$$

Simple manipulations of (13) and $H$ yield the following:

$$\begin{cases} -\dot{s}[\phi] + [\phi u] = 0 \\ -\dot{s}[\phi u] + [\phi u^2] = -\left[\frac{1}{2}\phi^2\right] - \frac{1}{2}(\phi_L^2 - \phi_s^2) \end{cases} \tag{15}$$

where according to the previous assumptions $h_L > h_R$, the quantity $\phi_s$ is defined as

$$\phi_s = \phi_L - g(h_L - h_R) \tag{16}$$

*2.2.1. Rankine–Hugoniot condition for $\dot{s} = 0$*

We are now in the position to write the conditions which must be satisfied across the characteristics, defined by the eigenvalue $\lambda_2$, along which the bottom remains constant. The complete Rankine–Hugoniot conditions for (1) are obtained from (15):

$$\begin{aligned} &-\dot{s}[\phi] + [\phi u] = 0 \\ &-\dot{s}[\phi u] + [\phi u^2] = -\left[\frac{1}{2}\phi^2\right] + \frac{1}{2}(\phi_L^2 - \phi_s^2) \\ &-\dot{s}[\phi v] + [\phi uv] = 0 \\ &-\dot{s}[h] = 0 \end{aligned}$$

where again $[h] = h_R - h_L$. The last equation implies that two situations are possible [11]: (a) the bottom function $h(x)$ remains constant across the shock, or (b) the bottom function $h(x)$ is discontinuous but the shock velocity vanishes. Case (b) applies when bottom discontinuities are present and the Rankine–Hugoniot conditions reduce to the following system:

$$\begin{aligned} &+[\phi u] = 0 \\ &+[\phi u^2] = -[\frac{1}{2}\phi^2] - \frac{1}{2}(\phi_L^2 - \phi_s^2) \\ &+[\phi uv] = 0 \end{aligned}$$

Using previous definitions the system can be expressed in terms of the left and right conditions. When $h_L > h_R$ we have:

$$\begin{aligned} &-\phi_L u_L + \phi_R u_R = 0 \\ &-\phi_L u_L^2 + \phi_R u_R^2 = \frac{1}{2}(\phi_L - g(h_L - h_R))^2 - \frac{1}{2}\phi_R^2 \\ &-\phi_L u_L v_L + \phi_R u_R v_R = 0 \end{aligned} \tag{17}$$

The situation is illustrated in Fig. 4. Eq. (17) represent the relation between the left and right states across a bottom discontinuity of the form of a step. That is, conditions (17) state that the left and right mass of water satisfy the conservation laws of mass and momentum flux across the bottom step. The uneven bottom acts as a cross-sectional variation in a pipe duct, where the pressure is constant across the changed section but the fluid equilibrium is achieved by the reaction of the solid wall of the pipe. This shows the particular nature of the fluid which can transmit the pressure unchanged by the modification of the mass flux [13].

We now use (17) to deduce the velocity before and after the step as a function of the total depth. First, we remark that due to the definition of $\phi_L$ and $\phi_R$, which are always positive quantities, the following lemmas hold:

**Lemma 2.1.** *The velocity $u_L$ and $u_R$ have the same sign.*

The proof is trivial and is thus omitted.

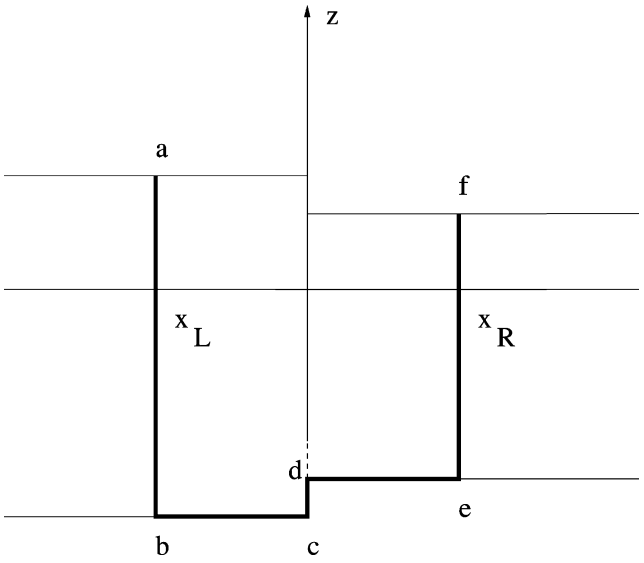


Fig. 4. Volume of fluid crossing the bottom change.

Now following the method used in [17] we define:

$$\phi_L u_L = \phi_R u_R = M$$

In the one-dimensional space used $M$ is the volume rate passing through the stationary shock by the gravity acceleration $g$. Now the second equation of (17) can be manipulated so as to obtain

$$M = \pm\sqrt{\frac{1}{2}\frac{\phi_L\phi_R}{\phi_L - \phi_R}\left(\left(\phi_L - g(h_L - h_r)\right)^2 - \phi_R^2\right)} \tag{18}$$

Using the previous relation for $M$ we can obtain the following expression for the velocities:

$$u_L = \pm\sqrt{\frac{1}{2}\frac{\phi_R}{\phi_L}\frac{\left(\phi_L - g(h_L - h_R)\right)^2 - \phi_R^2}{\phi_L - \phi_R}} \tag{19}$$

$$u_R = \pm\sqrt{\frac{1}{2}\frac{\phi_L}{\phi_R}\frac{\left(\phi_L - g(h_L - h_R)\right)^2 - \phi_R^2}{\phi_L - \phi_R}} \tag{20}$$

Let us define the non-dimensional quantities:

$$\varepsilon = \frac{\phi_R}{\phi_L}, \quad \mu = \frac{M}{\phi_L^{3/2}}, \quad \Delta h = \frac{g(h_L - h_R)}{\phi_L}$$

Then the relation between the non-dimensional volume flux $\mu$ and the non-dimensional total depth $\varepsilon$ becomes:

$$\mu = \pm\sqrt{\frac{1}{2}\varepsilon\frac{(1-\Delta h)^2 - \varepsilon^2}{1-\varepsilon}}$$

We now introduce the Froude numbers of the left and right states of the stationary shock as follows:

$$F_L = \frac{u_L}{\sqrt{\phi_L}}, \quad F_R = \frac{u_R}{\sqrt{\phi_R}}$$

which can be connected to the non-dimensional mass flux $\mu$ as follows:

$$F_L = \pm\sqrt{\frac{1}{2}\varepsilon\frac{(1-\Delta h)^2 - \varepsilon^2}{1-\varepsilon}}, \quad F_R = \pm\sqrt{\frac{1}{2\varepsilon^2}\frac{(1-\Delta h)^2 - \varepsilon^2}{1-\varepsilon}} \tag{21}$$

The quantities (21) exist when the expressions under the square root signs are greater than or equal zero

$$\frac{(1-\Delta h)^2-\varepsilon^2}{1-\varepsilon} \geqslant 0$$

The solution of the previous inequality leads to the following conditions:

$$\begin{cases} (1-\Delta h) \geqslant \varepsilon \\ 1 \geqslant \varepsilon \end{cases} \quad \text{or} \quad \begin{cases} (1-\Delta h) \leqslant \varepsilon \\ 1 \leqslant \varepsilon \end{cases} \tag{22}$$

Recall that $\Delta h \geqslant 0$. Also we must have $\phi_L \geqslant g(h_L - h_R)$, otherwise the total depth on the left side is lower than the step height and thus water cannot cross the step. Therefore, the inequalities reduce to two conditions which represent the domain of existence of Eq. (21):

$$(1-\Delta h) \geqslant \varepsilon \quad \text{and} \quad 1 \leqslant \varepsilon$$

In dimensional form the above inequalities read:

$$\begin{aligned} &\phi_L - g(h_L - h_R) \geqslant \phi_R, \qquad \phi_L \geqslant \phi_R \\ &\text{or} \\ &\phi_L \leqslant \phi_R \end{aligned} \tag{23}$$

The resulting graph of the two functions is shown in Fig. 5.

**Lemma 2.2.** *$F_L$ has two stationary points.*

**Proof.** The stationary points of $F_L$ are the roots of the following polynomial

$$P_1^3(\varepsilon) = 2\varepsilon^3 - 3\varepsilon^2 + (1-\Delta h)^2 \tag{24}$$

To find approximate values for the roots we use the perturbation technique of [2], which gives two meaningful positive roots in the form of a series expansion. The roots are:

$$\varepsilon_{sta,1} = 1 - \sqrt{\frac{2}{3}}\Delta h^{1/2} - \frac{2}{9}\Delta h + \frac{7}{54\sqrt{6}}\Delta h^{3/2} - \frac{5}{243}\Delta h^2 + O(\Delta h^{5/2}) \tag{25}$$

$$\varepsilon_{sta,2} = 1 + \sqrt{\frac{2}{3}}\Delta h^{1/2} - \frac{2}{9}\Delta h - \frac{7}{54\sqrt{6}}\Delta h^{3/2} - \frac{5}{243}\Delta h^2 + O(\Delta h^{5/2}) \qquad \square \tag{26}$$

**Lemma 2.3.** *The stationary points of $F_L$ coincide with the points at which the function $F_R$ is equal to* 1.

The proof is immediate and is thus omitted.

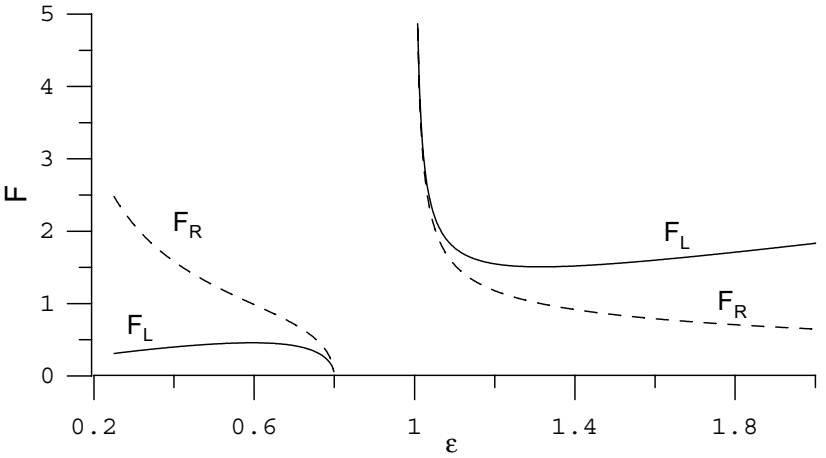


Fig. 5. Graphs of the Froude number for the left (solid line) and right (dashed line) states of the step for the case $\Delta h = 0.2$.

**Lemma 2.4.** *The left and right state variable vectors $U_L$ and $U_R$ cannot be identical except for an infinite value of the velocity.*

The proof is obvious and is thus omitted. In fact, it is obvious from Fig. 5 that the two curves corresponding to $F_L$ and $F_R$ values intersect only at $\varepsilon = 1$ with $F \to \infty$.

*2.2.2. Energy considerations for the Rankine–Hugoniot conditions*

In general, in addition to the system of Eq. (13) the condition that the energy of the fluid particles does not increase across the discontinuity must be satisfied. To apply this condition we again consider a fluid lying between two vertical planes. The total energy of water is given by:

$$T = \int_{x_L}^{x_R} E\,\mathrm{d}x + W$$

where $E$ is the column energy and $W(x)$ is the work of the external force

$$E = \frac{1}{2}\rho(\eta + h)u^2 + \frac{1}{2}\rho g(\eta^2 - h^2), \quad W = \int_{-h}^{\eta} p(x_L)u(x_L)\mathrm{d}t\,\mathrm{d}z - \int_{-h}^{\eta} p(x_R)u(x_R)\mathrm{d}t\,\mathrm{d}z$$

We note that our expression for $E$ differs from the usual expression given in [15] due to the different potential energy associated to columns of water at different bottom depths.

For the energy conservation theorem the following condition has to be satisfied together with Eq. (13):

$$\frac{\mathrm{d}}{\mathrm{d}t}T \leqslant 0 \tag{27}$$

where

$$\frac{\mathrm{d}}{\mathrm{d}t}T = \frac{\mathrm{d}}{\mathrm{d}t}\int_{x_L}^{x_R} E\,\mathrm{d}x + \int_{-h}^{\eta} p(x_L)u(x_L)\,\mathrm{d}z - \int_{-h}^{\eta} p(x_R)u(x_R)\,\mathrm{d}z$$

If we now consider a stationary shock condition, $\dot{s} = 0$, condition (27) should be satisfied together with (17). This would allow us to determine physically admissible states characterized by the ratio $\varepsilon$. In other words, we can rule out some possible solutions which are allowed by inequalities (23).

Without loss of generality we can set $h_R = 0$. After some algebraic manipulations we arrive at the following equation

$$\frac{g}{\rho}\frac{\mathrm{d}}{\mathrm{d}t}T = \frac{1}{2}M(u_R - u_L)(u_R + u_L) - \frac{1}{2}\phi_L(\phi_L - 2gh_L)u_L + \phi_R^2 u_R - \frac{1}{2}\phi_L^2 u_L$$

Using the second equation of (17) and the definition of $M$ the time derivative of the total energy can be written as

$$\frac{\mathrm{d}}{\mathrm{d}t}T = \frac{M}{4}\left(\frac{((\phi_L - gh_L)^2 - \phi_R^2)(\phi_L + \phi_R)}{\phi_L\phi_R} - 2(\phi_L - 2gh_L) + 4\phi_R - 2\phi_L\right) \tag{28}$$

**Lemma 2.5.** *The interval where $\frac{\mathrm{d}}{\mathrm{d}t}T \leqslant 0$ holds depends on the sign of the flux $M$.*

**Proof.** The right-hand side of (28) can be written in the following non-dimensional form:

$$\frac{\mu}{4\varepsilon}(-\varepsilon^3 + 3\varepsilon^2 + (-3 + 2\Delta h + \Delta h^2)\varepsilon + 1 - 2\Delta h + \Delta h^2) \tag{29}$$

It is obvious that the sign of $\mu/4\varepsilon$ is defined by that of $\mu$ and is proportional to $M$. Therefore, the sign of the non-dimensional expression for the total energy is related to the sign of the following third-order polynomial:

$$P^3(\varepsilon) = -\varepsilon^3 + 3\varepsilon^2 + (-3 + 2\Delta h + \Delta h^2)\varepsilon + 1 - 2\Delta h + \Delta h^2$$

In order to study the sign of the polynomial we first find its roots by doing a perturbation analysis in the neighborhood of $\Delta h = 0$. This case is a singular case for $P^3(\varepsilon)$, where the polynomial has one threefold root $\varepsilon = 1$. We again search for roots as a series expansion with respect to $\sqrt{h}$ and obtain the following expressions for the roots as a function of $\Delta h$:

$$\varepsilon_1 = 1 - \sqrt{2}\Delta h^{1/2} + \frac{\Delta h}{2} - \frac{\sqrt{2}}{16}\Delta h^{3/2} + \frac{\sqrt{2}}{512}\Delta h^2 + \frac{\sqrt{2}}{8192}\Delta h^3 + O(\Delta h^{7/2}) \tag{30}$$

$$\varepsilon_2 = 1 - \Delta h \tag{31}$$

$$\varepsilon_3 = 1 + \sqrt{2}\Delta h^{1/2} + \frac{\Delta h}{2} + \frac{\sqrt{2}}{16}\Delta h^{3/2} - \frac{\sqrt{2}}{512}\Delta h^2 + \frac{\sqrt{2}}{8192}\Delta h^3 + O(\Delta h^{7/2}) \tag{32}$$

It is worth noting that the second root is equal to the left boundary of the non-existence region of the velocity as given by (22). Looking at the sign of the polynomial $P^3(\varepsilon)$ in Fig. 6 we can now determine the regions where the energy dissipates. The admissible regions of $\varepsilon$ depend on the sign of the non-dimensional volume flux $\mu$ and are the following:

$$\mu > 0 : \varepsilon_1 < \varepsilon < \varepsilon_2 \quad \text{and} \quad \varepsilon_3 < \varepsilon$$

and

$$\mu < 0 : 0 < \varepsilon < \varepsilon_1 \quad \text{and} \quad 1 < \varepsilon < \varepsilon_3 \qquad \square$$

### 2.3. Gas dynamics analogy

The analogy between the equations of isentropic gas dynamics and the shallow water equations was noticed in [15] for the flat bottom case and one space dimension. It is of interest to see if such an analogy can be extended to the present system with a source term. The isentropic equations of gas dynamics in one space dimension can be written as follows:

$$\begin{aligned} &\frac{\partial \bar{\rho}}{\partial t} + \frac{\partial(\bar{\rho}u)}{\partial x} = 0 \\ &\frac{\partial(\bar{\rho}u)}{\partial t} + \frac{\partial}{\partial x}(\bar{\rho}u^2 + p(\bar{\rho})) = 0 \end{aligned} \tag{33}$$

where the pressure $p$ is connected to the density by the relation:

$$p = k\bar{\rho}^{\gamma}$$

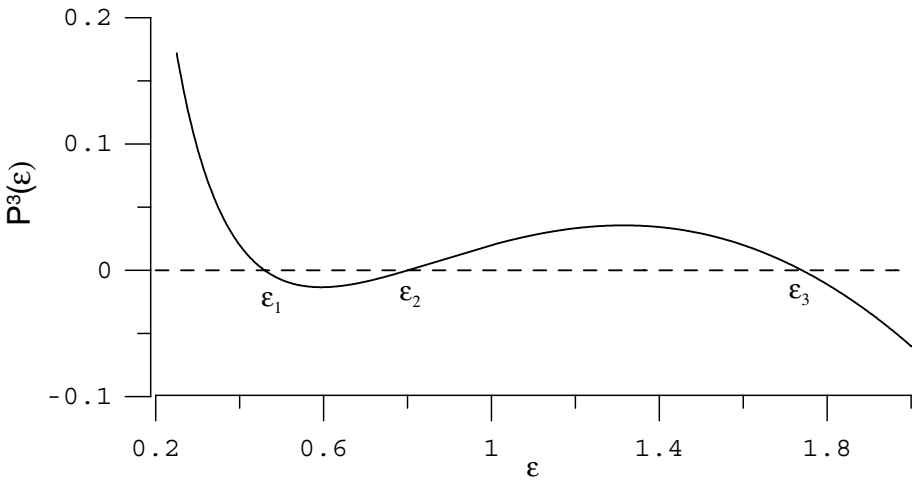


Fig. 6. Graph of the polynomial $P^3(\varepsilon)$.

The shallow water equations in one spatial dimension read:

$$\begin{aligned} &\frac{\partial}{\partial t}(gd) + \frac{\partial}{\partial x}(gdu) = 0 \\ &\frac{\partial}{\partial t}(gdu) + \frac{\partial}{\partial x}(gdu^2 + \frac{1}{2}(gd)^2) = 0 \end{aligned} \tag{34}$$

We now define the following quantities

$$\bar{\rho} = d, \quad p = kd^{\gamma}, \quad k = \frac{1}{2}, \quad \gamma = 2$$

With the above notation, systems (34) and (33) are identical.

When the cross-sectional area of the gas tube is not constant, a source term appears and (33) is modified as follows:

$$\begin{aligned} &\frac{\partial(a\bar{\rho})}{\partial t} + \frac{\partial(a\bar{\rho}u)}{\partial x} = 0 \\ &\frac{\partial(a\bar{\rho}u)}{\partial t} + \frac{\partial}{\partial x}(a\bar{\rho}u^2 + ap(\bar{\rho})) = p(\bar{\rho})\frac{\partial a}{\partial x} \\ &\frac{\partial a}{\partial t} = 0 \end{aligned} \tag{35}$$

where $a(x)$ is the cross-sectional area and

$$p(\bar{\rho}) = k\frac{\gamma}{\gamma - 1}\bar{\rho}^{\gamma - 1}$$

The one-dimensional shallow water equations with variable bottom read:

$$\begin{aligned} &\frac{\partial}{\partial t}(gd) + \frac{\partial}{\partial x}(gdu) = 0 \\ &\frac{\partial}{\partial t}(gdu) + \frac{\partial}{\partial x}(gdu^2 + \frac{1}{2}(gd)^2) = g(gd)\frac{\partial h}{\partial x} \\ &\frac{\partial h}{\partial t} = 0 \end{aligned} \tag{36}$$

It is clear that due to the difference in the momentum conservation equation no analogy exists between (35) and (36). One may argue that when a piecewise constant bottom and a piecewise constant cross-sectional area are used then analogy can be restated. In fact as previously discussed at the end of Section 2.1 and in [11] (where $a(x)$ and $h(x)$ are piecewise constant), systems (35) and (36) are identical to (33) and (34), respectively. The differences arise in the discontinuity points for the bottom and for the cross-sectional area. In fact, following the discussion in [11], the Rankine–Hugoniot conditions, associated with the last equation of systems (35) and (36), takes the following form:

$$\lambda[a] = 0$$

When the cross-sectional area/bottom is discontinuous the associated eigenvalue must be zero, $\lambda = 0$, and following [11] we can rewrite (35) in conservative form and obtain the following Rankine Hugoniot conditions at the step:

$$\begin{aligned} &[a\bar{\rho}u] = 0 \\ &\left[\frac{u^2}{2} + p'(\bar{\rho})\right] = 0 \end{aligned} \tag{37}$$

In the case of the shallow water equations no conservative form is available and the Rankine–Hugoniot conditions for the first two equations are given by:

$$\begin{aligned} &[gdu] = 0 \\ &\left[gdu^2 + \frac{1}{2}(gd)^2\right] = +H \end{aligned} \tag{38}$$

It is obvious that the conditions expressed by (37) and (38) are different.

## 3. Solution of the Riemann problem with a bottom step

In this section we construct the solution of the Riemann problem for (1) with piecewise constant initial data represented by $U_L$, $U_R$. The solution of the Riemann problem, as depicted in Fig. 7, is represented by various regions of constant values of $u$ and $\phi$ separated by shock waves or rarefaction waves (see Fig. 8). In the present case, four different states are possible: $U_L(u_L, \phi_L)$, $U_R(u_R, \phi_R)$ – left and right initial data, $U_{L*}(u_{L*}, \phi_{L*})$ – the transition state between the 1-wave curve and the state to the left of the stationary wave (the step), $U_{R*}(u_{R*}, \phi_{R*})$ – the transition state between the state to the right of the stationary wave (the step) and the 3-wave curve.

An $n$-Wave is a shock or rarefaction wave in which the left and right states are connected by relations using the $n$-th eigenvalue and associated eigenvector of the hyperbolic Eq. (1). Such relations are the Rankine–Hugoniot conditions derived in Section 2.1 and the standard wave relations for the conventional shallow water equations [17]. We now consider the phase plane $(u - \phi)$. In the plane each point $U$ with coordinates $(u, \phi)$ represents the dynamic state of a vertical column of flow. If the velocity $u$ on the right of an $n$-Wave

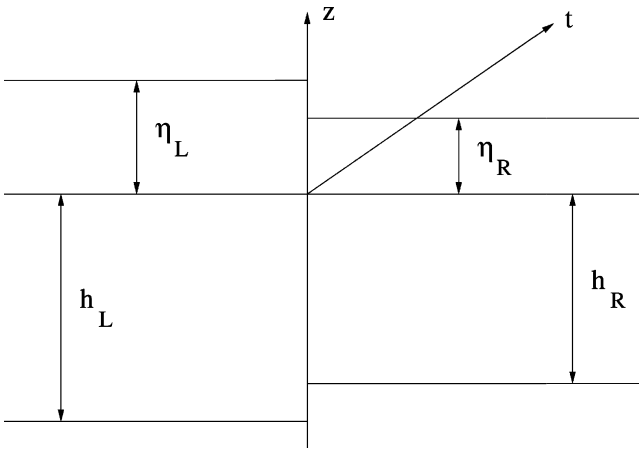


Fig. 7. Initial condition for the local RP.

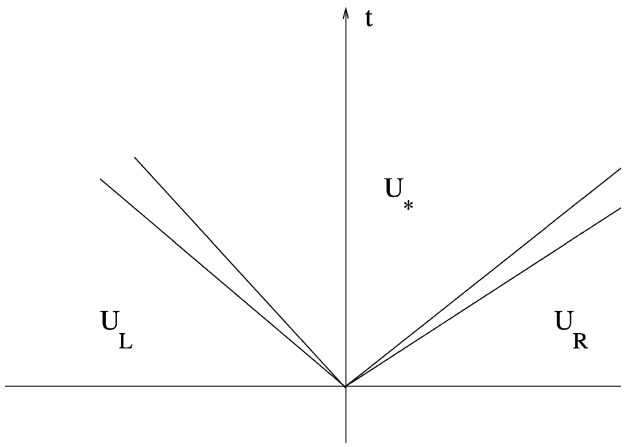


Fig. 8. wave patterns of the RP.

(either shock or rarefaction) is expressed as a function of the value of $\phi_{L*}$ on the same side and of the state on the left of the wave, then considering a 1-wave, the function $u_{L*}(U_L, \phi_{L*})$ determines a curve on the phase plane. Each point on the curve represents the right state of the corresponding 1-Wave while $U_L$ is the left state. The end points of the piecewise curve described connecting patches of the three curves (obtained by the three $n$-Wave families) represent the initial condition and the intersecting points, the transition states. In the following three subsections the possible interaction between the three different types of existing waves are analyzed and then, on this basis, the solution of the Riemann problem is constructed.

### 3.1. 1-Wave family curve

As seen in Section 2.1 the 1-Wave family curve corresponds to the 1-Wave family of the conventional shallow water equations without the fourth equation for a source term included. For given initial data of the left state and assuming that the total depth of the right state is known, the velocity of the right state of the wave is completely determined and is given by [17]:

$$u_{L*}(U_L, \phi_{L*}) = \omega_1(U_L, \phi_{L*}) = \begin{cases} u_L - 2\left(\sqrt{\phi_{L*}} - \sqrt{\phi_L}\right), & \phi_{L*} \leqslant \phi_L \\ u_L - (\phi_{L*} - \phi_L)\sqrt{\frac{(\phi_{L*}+\phi_L)}{2\phi_{L*}\cdot\phi_L}}, & \phi_{L*} \geqslant \phi_L \end{cases} \tag{39}$$

Here $U_L$ is the variable vector of the left state whereas $u_{L*}$ and $\phi_{L*}$ are the velocity and the square of the right celerity of the right state. Eq. (39) can be used for a graphical representation of the function $\omega_1$ (the ordinate of the point $(\phi, u)$) in the phase plane.

**Lemma 3.1.** *$\omega_1(U_L, \phi_{L*})$ is a non-increasing function of $\phi_{L*}$*

The proof is omitted.

### 3.2. 2-Wave family curve

The 2-Wave family curve called $\omega_2$ is drawn, in the phase plane, by the point $(u, \phi)$ whose coordinates $u$ and $\phi$ are the quantities at the right state of the stationary shock. For a given left state $(u_0, \phi_0)$ of the stationary shock, the velocity $u$ at the right is expressed by:

$$u_{R*}(U_{L*}, \phi_{R*}) = \omega_2(U_{L*}, \phi_{R*}) = \pm\sqrt{\frac{1}{2}\frac{\phi_{L*}}{\phi_{R*}}\frac{(\phi_{L*} - g(h_L - h_R))^2 - \phi_{R*}^2}{\phi_{L*} - \phi_{R*}}} \tag{40}$$

**Lemma 3.2.** *The function $\omega_2(U_{L*}, \phi_{R*})$ is always decreasing for the positive branch and always increasing for negative branch in $\phi_{R*}$.*

The proof is omitted.

On the other hand, if the 2-Wave is crossed from right to left, then the velocity of the left state is given by (19):

$$u_{L*} = \omega_2(\overleftarrow{\phi_{L*}, \phi_{R*}}) = \sqrt{\frac{1}{2}\frac{\phi_{R*}}{\phi_{L*}}\frac{(\phi_{L*} - g(h_L - h_R))^2 - \phi_{R*}^2}{\phi_{L*} - \phi_{R*}}} \tag{41}$$

From Section 2.2.1 the admissible values of $\phi$, for both Eqs. (39) and( 40) are given by the following inequalities:

$$0 < \phi_{R*} \leqslant \phi_{L*} - g(h_L - h_R) \quad \phi_{L*} < \phi_{R*}$$

We now study possible connections between the 1-Wave and 2-Wave family curves.

**Definition.** A point $(u_{R*}, \phi_{R*})$ is the conjugate of $(u_{L*}, \phi_{L*})$ if their coordinates are connected by (17)

**Definition.** Two curves $\omega_2(\phi_{L*}, \phi_{R*})$ and $\omega_1(U_L, \phi_{L*})$ are conjugate if all points $(u_{R*}, \phi_{R*})$ of $\omega_2$ are conjugate, one to one, to the points $(u_{L*}, \phi_{L*})$ of $\omega_1(U_L, \phi_{L*})$.

**Lemma 3.3.** *If two curves $\omega_1$ and $\omega_2$ are conjugate then the following condition holds*:

$$\Sigma_{1,2}(U_L, U_{L*}, \phi_{R*}) = \omega_2(\overleftarrow{\phi_{L*}, \phi_{R*}}) - \omega_1(U_L, \phi_{L*}) = 0 \tag{42}$$

**Proof.** If $\omega_2$ is the conjugate of $\omega_1$ then the point $(\omega_1(U_L, \phi_{L*}), \phi_{L*})$ represents the left state of a stationary shock and $\omega_1(U_L, \phi_{L*})$ is the velocity on the left of the stationary shock. The left velocity is also given by (41). □

**Lemma 3.4.** *There exist two values of $\phi_{R*}$ for which $\Sigma_{1,2}(U_L, U_{L*}, \phi_{R*}) = 0$.*

**Proof.** In the range $0 < \phi_{R*} \leqslant \phi_{L*} - g(h_L - h_R)$ we have:

$$\Sigma_{1,2}(U_L, U_{L*}, 0) = -\omega_1(U_L, \phi_{L*})$$
$$\Sigma_{1,2}(U_L, U_{L*}, \phi_{L*} - g(h_L - h_R)) = -\omega_1(U_L, \phi_{L*})$$

The function $\Sigma$ is continuous and is not identically constant. Therefore, the lemma is proven if we can show that the function has a stationary point inside the interval $0 < \phi_{R*} \leqslant \phi_{L*} - g(h_L - h_R)$. Using the result of Lemma 2.2 the point $\phi_{R*} = \varepsilon_{sta,1}\phi_{L*}$ is a stationary point for $\omega_2(\overleftarrow{\phi_{L*}, \phi_{R*}})$ inside the interval $0 < \phi_{R*} \leqslant \phi_{L*} - g(h_L - h_R)$. On the other hand, in the interval $\phi_{L*} < \phi_{R*}$ we have

$$\Sigma_{1,2}(U_L, U_{L*}, \phi_{L*}) \to +\infty, \quad \Sigma_{1,2}(U_L, U_{L*}, \infty) \to +\infty$$

Using the result of Lemma 2.2 the point $\phi_{R*} = \varepsilon_{sta,2}\phi_{L*}$ is a stationary point for $\omega_2(\overleftarrow{\phi_{L*}, \phi_{R*}})$ for $\phi_{L*} < \phi_{R*}$. □

Lemma 3.4 shows that for each $\omega_2$ curve there can be two possible conjugate curves $\omega_1$. That is, for each right state on the step there are two possible left states $U_L$. Similar non-uniqueness has been observed for other hyperbolic problems by other authors [11,9]. We now use Lemmas 2.1 and 2.5 to reduce non-uniqueness to a more narrow range.

**Lemma 3.5.** *In order to satisfy the energy dissipation condition the curve $\omega_2$ has to be split into positive and negative branches as follows*

$$\omega_2(U_{L*}, \phi_{R*}) = -\sqrt{\frac{1}{2}\frac{\phi_{L*}}{\phi_{R*}}\frac{(\phi_{L*} - g(h_L - h_R))^2 - \phi_{R*}^2}{\phi_{L*} - \phi_{R*}}}, \quad 0 < \frac{\phi_{R*}}{\phi_{L*}} < \varepsilon_1$$

$$\omega_2(U_{L*}, \phi_{R*}) = +\sqrt{\frac{1}{2}\frac{\phi_{L*}}{\phi_{R*}}\frac{(\phi_{L*} - g(h_L - h_R))^2 - \phi_{R*}^2}{\phi_{L*} - \phi_{R*}}}, \quad \varepsilon_1 < \frac{\phi_{R*}}{\phi_{L*}} < \varepsilon_2$$

$$\omega_2(U_{L*}, \phi_{R*}) = -\sqrt{\frac{1}{2}\frac{\phi_{L*}}{\phi_{R*}}\frac{(\phi_{L*} - g(h_L - h_R))^2 - \phi_{R*}^2}{\phi_{L*} - \phi_{R*}}}, \quad 1 < \frac{\phi_{R*}}{\phi_{L*}} < \varepsilon_3$$

$$\omega_2(U_{L*}, \phi_{R*}) = +\sqrt{\frac{1}{2}\frac{\phi_{L*}}{\phi_{R*}}\frac{(\phi_{L*} - g(h_L - h_R))^2 - \phi_{R*}^2}{\phi_{L*} - \phi_{R*}}}, \quad \varepsilon_3 < \frac{\phi_{R*}}{\phi_{L*}}$$

The proof is trivial and is based on Lemmas 2.1 and 2.5.

Fig. 9 shows plots of the non-dimensional curves $\omega_2(U_{L*}, \phi_{R*})$ and $\omega_2(\overleftarrow{\phi_{L*}, \phi_{R*}})$, denoted by $F_{R*}$ and $F_{L*}$, respectively. As is seen from the plot, the solution is still non-unique in the two regions: $\varepsilon_1 < \varepsilon < 1 - \Delta h$, due to the presence of $\varepsilon_{sta,1}$, and in $1 < \varepsilon < \varepsilon_3$, due to the presence of $\varepsilon_{sta,2}$. It is worth noting that when $\phi_{R*}$ moves inside these intervals the value of $F_{R*}$ crosses the $F = 1$ line (see Fig. 9), which corresponds to moving from a supercritical state to a subcritical one (or vice versa). In fact, from $F = 1$ (where $F$ is the Froude number of the right state of the stationary shock) follows that $u = \sqrt{\phi}$. If we define, in the phase plane, the critical state curve $C$ by the equation:

$$u = \pm\sqrt{\phi}$$

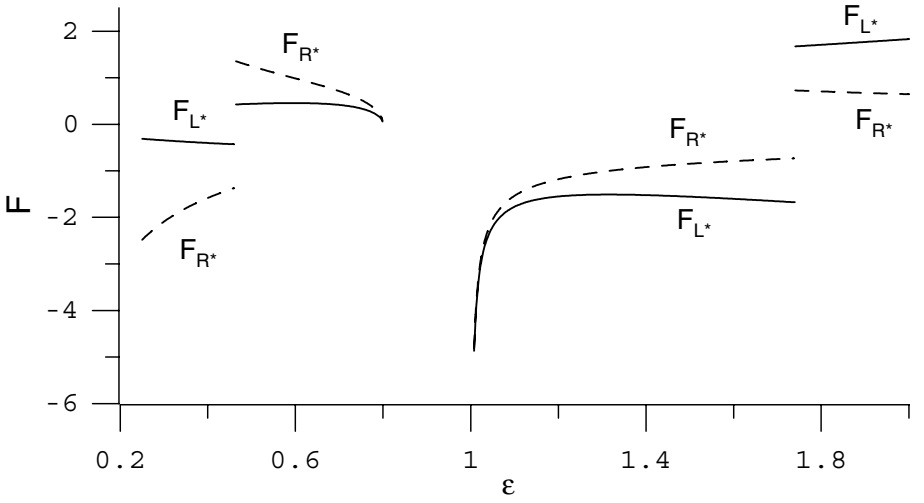


Fig. 9. Plots of the left and right Froude numbers at the step.

then we can see that for the values of $\phi$ in the above intervals of non-uniqueness the corresponding 2-Wave family curve $\omega_2(U_{L*}, \phi)$ crosses the critical state curve $C$, changing the right state of the wave from a subcritical one to a supercritical one (or vice versa). If we define

$$F_{\max} = F_L(\varepsilon_{sta,1}), \quad F_{\min} = F_L(\varepsilon_{sta,2})$$

and $C_{\max}$ and $C_{\min}$ are the curves corresponding to the equations

$$u' = \pm F_{\max}\sqrt{\phi_{L*}}, \quad u' = \pm F_{\min}\sqrt{\phi_{L*}}$$

respectively, we can draw the following conclusion from the analysis of Fig. 9: no values of $F$ are allowed in the region $|F_{\max}| < |F| < |F_{\min}|$ and therefore the representative point $(u_{L*}, \phi_{L*})$ of the left state cannot be inside the two regions defined by curves $C_{\max}$ and $C_{\min}$. Thus, the critical state curve is internal to the domain bounded by $C_{\max}$ and $C_{\min}$.

As a result of the previous observations and Lemma 2.3 we can say that the crossing of the unity value by $F_{R*}$ corresponds to the change of sign for the derivative of $F_{L*}$. The non-uniqueness can be avoided if we require that the curve $\omega_2(\overleftarrow{\phi_{L*}, \phi_{R*}})$ be always decreasing in the positive branch and increasing in the negative one. This approach can be compared to the monotonicity criterion presented by [11]. There, the monotonicity criterion is equivalent to requiring that no stationary shock crosses the boundary of hyperbolicity, which corresponds here to the critical state curve. The mathematical meaning of crossing is that the system of equations (1) is no longer hyperbolic when the representative point $(u, \phi)$ of the curve $\omega_2(U_{L*}, \phi_{R*})$ is on the critical state curve. We now modify the definition of curve $\omega_2(U_{L*}, \phi_{R*})$ in Lemma 3.5 as follows:

$$\begin{aligned}
\omega_2(U_{L*}, \phi_{R*}) &= -\sqrt{\frac{1}{2}\frac{\phi_{L*}}{\phi_{R*}}\frac{(\phi_{L*} - g(h_L - h_R))^2 - \phi_{R*}^2}{\phi_{L*} - \phi_{R*}}}, \quad 0 < \frac{\phi_{R*}}{\phi_{L*}} < \varepsilon_1 \\
\omega_2(U_{L*}, \phi_{R*}) &= \sqrt{\frac{1}{2}\frac{\phi_{L*}}{\phi_{R*}}\frac{(\phi_{L*} - g(h_L - h_R))^2 - \phi_{R*}^2}{\phi_{L*} - \phi_{R*}}}, \quad \varepsilon_{sta,1} < \frac{\phi_{R*}}{\phi_{L*}} < \varepsilon_2 \\
\omega_2(U_{L*}, \phi_{R*}) &= -\sqrt{\frac{1}{2}\frac{\phi_{L*}}{\phi_{R*}}\frac{(\phi_{L*} - g(h_L - h_R))^2 - \phi_{R*}^2}{\phi_{L*} - \phi}}, \quad 1 < \frac{\phi_{R*}}{\phi_{L*}} < \varepsilon_{sta,2} \\
\omega_2(U_{L*}, \phi_{R*}) &= \sqrt{\frac{1}{2}\frac{\phi_{L*}}{\phi_{R*}}\frac{(\phi_{L*} - g(h_L - h_R))^2 - \phi_{R*}^2}{\phi_{L*} - \phi_{R*}}}, \quad \varepsilon_3 < \frac{\phi_{R*}}{\phi_{L*}}
\end{aligned} \tag{43}$$

Now it is possible to look for the solution of (42) in connection with the left conditions of the Riemann problem. To this end we introduce the following non-dimensional quantities:

$$\gamma_L = \frac{\phi_L}{\phi_{L*}}, \quad F_L = \frac{u_L}{\sqrt{\phi_L}}, \quad \varepsilon = \frac{\phi_{R*}}{\phi_{L*}}$$

Then $\Sigma_{1,2}$ can be rewritten in the non-dimensional form as follows:

$$\sigma_{1,2} = \begin{cases} F_{L*}(\varepsilon) - \sqrt{\gamma_L} F_L + (1-\gamma_L)\sqrt{\frac{1+\gamma_L}{2\gamma_L}}, & \gamma_L < 1 \\ F_{L*}(\varepsilon) - \sqrt{\gamma_L} F_L + 2(1-\sqrt{\gamma_L}), & \gamma_L \geqslant 1 \end{cases} \tag{44}$$

where

$$F_{L*}(\varepsilon) = \pm\sqrt{\frac{1}{2}\varepsilon\frac{(1-\Delta h)^2 - \varepsilon^2}{1-\varepsilon}}$$

The sign of the square root is defined by $\varepsilon$ according to Lemma 3.5. Now Eq. (42) in non-dimensional form reads:

$$\sigma_{1,2} = 0 \tag{45}$$

which is a relation between $\varepsilon$ and $\gamma_L$. For each value of $\varepsilon$ Eq. (45) determines the value of $\gamma_L$ providing information about the left state of the Riemann problem.

**Lemma 3.6.** *If $F_{L*} - F_L \geqslant 0$ and $F_L \geqslant -2$ the solution of Eq. (45) exists, is unique and is contained inside the interval $1 \leqslant \gamma_L$.*

**Proof.** When $1 \leqslant \gamma_L$ we obtain from (44): the following expression for $\gamma_L$:

$$\gamma_L = \left(\frac{F_{L*}+2}{F_L+2}\right)^2 \tag{46}$$

If $1 \leqslant \gamma_L$ holds then it can be shown that

$$\frac{F_{L*} - F_L}{F_L + 2} \geqslant 0$$

The previous inequality is true for:

$$\begin{cases} F_{L*} - F_L \geqslant 0 \\ F_L > -2 \end{cases} \quad \begin{cases} F_{L*} - F_L \leqslant 0 \\ F_L < -2 \end{cases} \qquad \square$$

**Lemma 3.7.** *For $\gamma_L < 1$ and $F_L > -2$ we have $\frac{\partial \sigma_{1,2}}{\partial \gamma_L} < 0$ and the function $\sigma_{1,2}$ is monotone in $\gamma_L$ in the same interval.*

**Proof.** We need to study the sign of the derivative of $\sigma_{1,2}$ with respect to $\gamma_L$ in the region $\gamma_L < 1$. The derivative is given by

$$\frac{d\sigma_{1,2}}{d\gamma_L} = \frac{-\sqrt{2}(1+\gamma_L+2\gamma_L^2) - 2F_L\gamma_L^{3/2}\sqrt{\frac{1+\gamma_L}{\gamma_L}}}{4\gamma_L^2\sqrt{\frac{1+\gamma_L}{\gamma_L}}}$$

Since the denominator is always positive the sign of the derivative depends on the sign of the numerator only. The numerator is negative if

$$-\frac{1+\gamma_L+2\gamma_L^2}{\sqrt{\gamma_L^2(1+\gamma_L)}} < \frac{2F_L}{\sqrt{2}}$$

The left-hand side is monotone for $0 < \gamma_L < 1$ and attains its maximum at $\gamma_L = 1$. Therefore, the following inequality holds:

$$-\frac{1+\gamma_L+2\gamma_L^2}{\sqrt{\gamma_L^2(1+\gamma_L)}} < -\frac{4}{\sqrt{2}} < \frac{2F_L}{\sqrt{2}}$$

which gives $-2 < F_L$. □

**Lemma 3.8.** *Let $F_{L*} - F_L < 0$. Then if $F_L > -2$ the solution of (45) exists, is unique and is contained inside the interval $0 < \gamma_L < 1$, whereas if $F_L < -2$ the solution exists, is unique and is in the interval $1 \leqslant \gamma_L$.*

The proof is omitted.

We know that for $F_{L*} - F_L > 0$ and $F_L < -2$ no solution exists. This situation corresponds to the generation of a dry zone on the left side of the Riemann problem, so the solution must have a different structure. In fact, if $F_L < -2$ then from $F' - F_L > 0$ it follows that a rarefaction fan connects the left side condition with the right condition of the 1-Wave, but the velocity of the left fluid is larger than the maximum velocity the rarefaction fan can connect.

A summary of the previous discussion is as follows: for physically meaningful data it is possible to uniquely join a 1-Wave curve with a 2-Wave curve connecting the left initial data of the Riemann problem with the state on the right side of the step.

### 3.3. 3-Wave family curve

The 3-Wave family curve corresponds to a 2-Wave family of the shallow water equations without a source term; we choose to call it a "3-Wave" to avoid confusion in the final system solution. We now cross the wave from right to left. For a given initial right state of the wave denoted by $U_0$ the velocity on the left of the wave is given by [17]:

$$u_{R*}(U_R, \phi_{R*}) = \overleftarrow{\omega_3}(U_R, \phi_{R*}) = \begin{cases} u_R + 2\left(\sqrt{\phi_{R*}} - \sqrt{\phi_R}\right), & \phi_{R*} \leqslant \phi_R \\ u_R + (\phi_{R*} - \phi_R)\sqrt{\frac{(\phi_{R*}+\phi_R)}{2\phi_{R*}\phi_R}}, & \phi_{R*} \geqslant \phi_R \end{cases} \tag{47}$$

As in Section 3.1, we now study the properties of the curve.

**Lemma 3.9.** *$\overleftarrow{\omega_3}(U_R, \phi_{R*})$ is an increasing function of $\phi_{R*}$.*

The proof is similar to that of Lemma 3.1 and is thus omitted.

For a 3-Wave family curve, defined by (47), there exists a straightforward graphical interpretation of its composition with a 2-Wave family curve: the point $(u, \phi)$ is the intersection between $\overleftarrow{\omega_3}(U_R, \phi_{R*})$ and $\omega_2(U_{L*}, \phi_{R*})$. If we define

$$\Sigma_{2,3}(U_{L*}, U_R, \phi_{R*}) = \overleftarrow{\omega_3}(U_R, \phi_{R*}) - \omega_2(U_{L*}, \phi_{R*})$$

the condition of intersection is expressed by the following equation:

$$\Sigma_{2,3}(U_{L*}, U_R, \phi_{R*}) = 0 \tag{48}$$

Similar to the previous discussion, we define the following non-dimensional quantities:

$$\gamma_R = \frac{\phi_R}{\phi_{L*}}, \quad F_R = \frac{u_R}{\sqrt{\phi_R}}$$

Then the curves $\omega_2$ and $\overleftarrow{\omega_3}$ can be expressed in non-dimensional form as follows:

$$\sigma_{2,3} = \begin{cases} \pm\sqrt{\frac{1}{2\varepsilon}\frac{(1-\Delta h)^2-\varepsilon^2}{1-\varepsilon}} - \sqrt{\gamma_R}F_R - (\varepsilon - \gamma_R)\sqrt{\frac{\varepsilon+\gamma_R}{2\varepsilon\gamma_R}}, & \gamma_R < \varepsilon \\ \pm\sqrt{\frac{1}{2\varepsilon}\frac{(1-\Delta h)^2-\varepsilon^2}{1-\varepsilon}} - \sqrt{\gamma_R}F_R - 2(\sqrt{\varepsilon} - \sqrt{\gamma_R}), & \varepsilon \leqslant \gamma_R \end{cases} \tag{49}$$

Recalling (21) we again define:

$$\sqrt{\varepsilon}F_{L*}(\varepsilon) = \pm\sqrt{\frac{1}{2\varepsilon}\frac{(1-\Delta h)^2-\varepsilon^2}{1-\varepsilon}}$$

Then (48) takes the following form:

$$\sigma_{2,3} = 0 \tag{50}$$

**Lemma 3.10.** *For $F_{L*} - F_R \leqslant 0$ and $F_R \leqslant 2$ the solution of (50) exists, is unique and is contained in the interval $\varepsilon \leqslant \gamma_R$.*

**Proof.** When $\varepsilon \leqslant \gamma_L$ from (49) we obtain the following expression for $\gamma_R$:

$$\gamma_R = \varepsilon\left(\frac{F_{L*} - 2}{F_R - 2}\right)^2 \tag{51}$$

If $\varepsilon \leqslant \gamma_L$ holds then we have the following conditions

$$\begin{cases} F_{L*} - F_R \leqslant 0 \\ F_R \leqslant 2 \end{cases} \quad \begin{cases} F_{L*} - F_R \geqslant 0 \\ F_R \geqslant 2 \end{cases} \qquad \square$$

**Lemma 3.11.** *For $\gamma_R < \varepsilon$ and $F_R < 2$ we have $\frac{\partial \sigma_{2,3}}{\partial \gamma_R} > 0$ and the function $\sigma_{2,3}$ is monotone in the same interval.*

The proof is similar to that for the 1-Wave and is thus omitted.

**Lemma 3.12.** *Let $F_{L*} - F_R \geqslant 0$. Then for $F_R < 2$ the solution of (50) exists, is unique and is contained in the interval $0 \leqslant \gamma_R < \varepsilon$, whereas for $F_R > 2$ the solution exists, is unique and is in the interval $\varepsilon \leqslant \gamma_R$.*

The proof is omitted.

We remark that for $F_{L*} - \sqrt{\varepsilon} F_R \leqslant 0$ and $F_R > 2$ no physically meaningful solution exists due to the same reasons given in Section 3.2. The velocity on the right state generates a dry-bed condition because it is above the maximum velocity the 3-wave fan can adjust to.

In conclusion, Lemmas 3.6, and 3.8, 3.10, and 3.12 demonstrate the way of constructing a path in the phase plane connecting the left and right initial conditions.

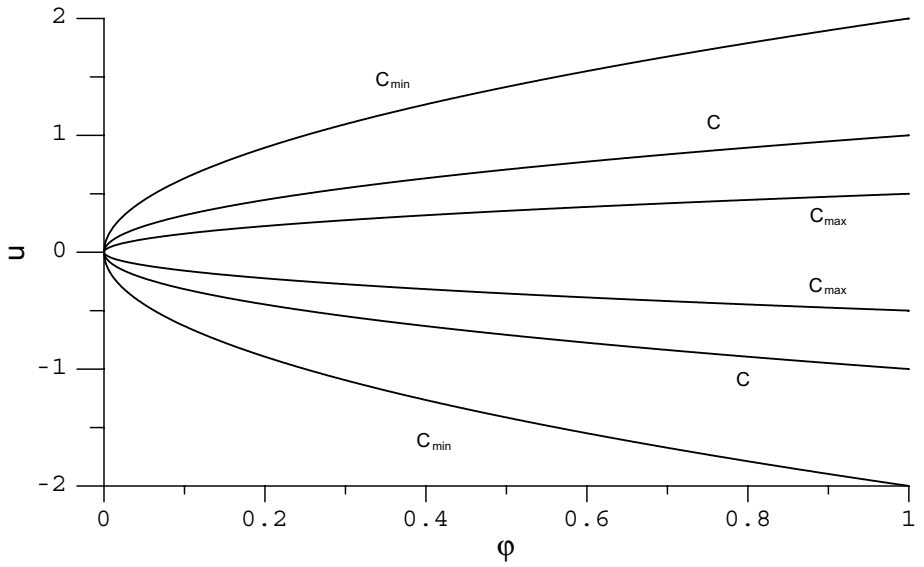


Fig. 10. Sketch of the critical curve in the phase plane.

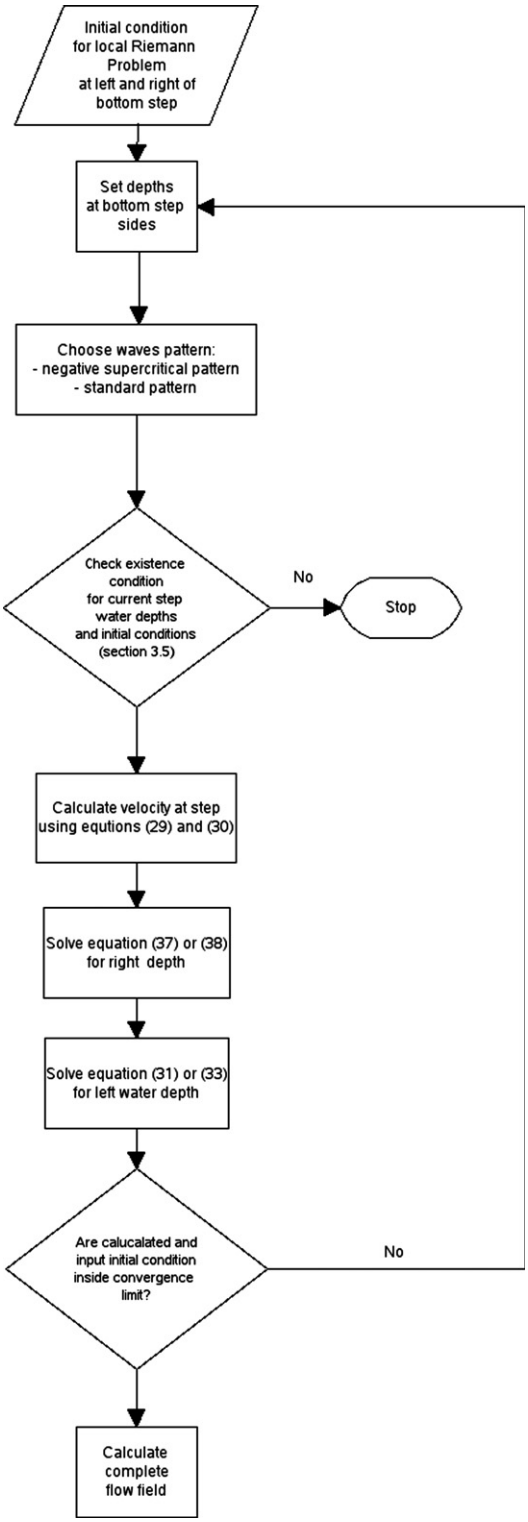


Fig. 11. Flow chart of the solution procedure of the local Riemann Problem.

### 3.4. Conditions on the wave patterns

The conclusions in the previous sections give arguments for the existence and uniqueness of the solution, hence the possibility to draw a path in the phase plane connecting the representative point of the left state to the one representing the right state of the Riemann problem. The resulting solution is bounded by some conditions implicitly expressed by (21). These conditions are graphically represented in Fig. 10, where it is possible to see that no point, representative of the state on the left of a stationary shock, can lie between the curves $C_{\mathrm{MAX}}$ and $C_{\mathrm{MIN}}$. This fact implies that some wave configurations cannot be allowed.

**Lemma 3.13.** *A wave pattern in which a* 1*-Wave shock overcomes a* 2*-Wave is not possible.*

**Proof.** If a 1-Wave overcome a 2-Wave the shock velocity has to be positive $\dot{s}_1 > 0$ then and for the Lax inequalities $F_{\mathrm{L}*} > 1$. The condition for $F_{\mathrm{L}*}$ holds only for $\varepsilon > \varepsilon_3$ and in this interval $F < 1$ then $\lambda_1(u, \phi) < 0$. From the Lax inequalities

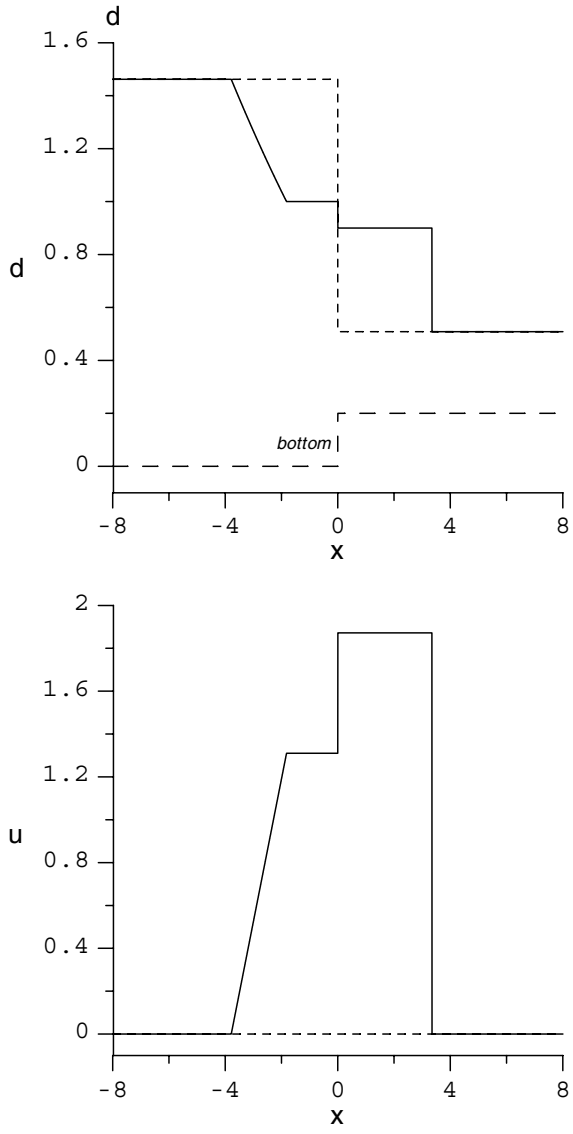


Fig. 12. Graphs of the total depth and mean velocity for the dam-breaking case.

$$0 > \lambda_1(u, \phi) > \dot{s} > \lambda_1(u_R, \phi_R) \tag{52}$$

which contradict the initial assumption. □

**Lemma 3.14.** *A wave pattern in which a* 3*-Wave shock overcomes, in the second quadrant, a* 2*-Wave is not possible for* $0 \leqslant \varepsilon \leqslant \varepsilon_1$.

**Proof.** If a 3-Wave curve is in the second quadrant we then have $\dot{s} \leqslant 0$, meaning that

$$\lambda_3(U_{L*}) < \dot{s} < 0$$

This condition is compatible with the values of $F < -1$. In the interval of interest the value of $F_{L*} > -1$ corresponds to $F < -1$, hence

$$0 < \lambda_3(U_{L*})$$

which contradicts the assertion. □

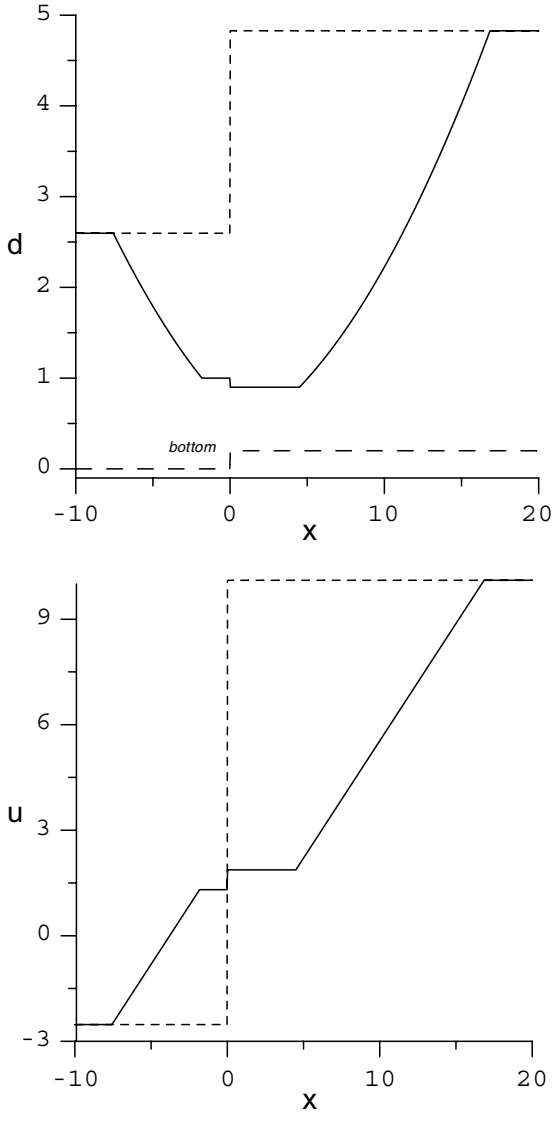


Fig. 13. Graphs of the total depth (a) and mean velocity (b) for the two rarefaction case.

**Lemma 3.15.** *A rarefaction fan containing the stationary shock is not allowed.*

**Proof.** If a rarefaction fan contains the $t$ axis (the stationary shock) then the left state of the stationary shock must have $F_{L*} = 1$, which is is not compatible with the function $\omega_2(\overleftarrow{\phi_{L*}, \phi_{R*}})$ □

According to the previous lemmas the only possible alternative allowable pattern is to have two subcritical 1-Wave and 3-Wave (wave in the second quadrant of the $x - t$ plane) and a stationary shock, for $\varepsilon$ values inside the interval $1 < \varepsilon < \varepsilon_{sta,2}$. In fact in this case the subcritical motion started at the right side of the step is extended to the left side as the graph of $F\prime$ in Fig. 9 shows. There is a physical reason to support this: the step acts as a reflecting mechanism on the signal incoming from the left and forcing the presence of a 1-Wave in the second quadrant in the presence of supercritical motion too. On the other hand, when there is a subcritical motion from the right of the step there is no reason for a reflection turning in the first quadrant the 3-Wave, so it can extend to the second quadrant.

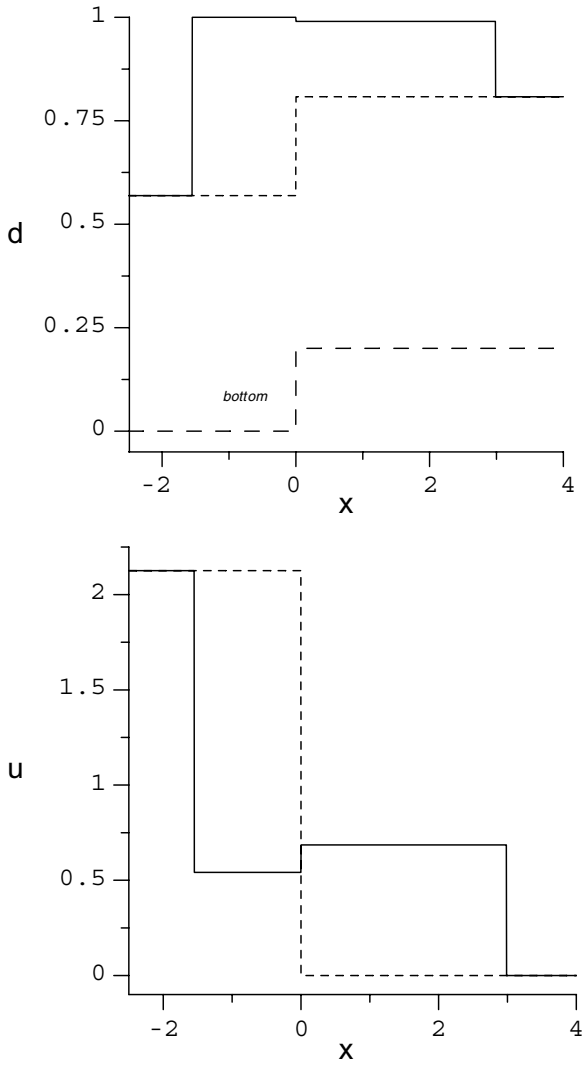


Fig. 14. Graphs of the total depth and mean velocity for the two shock case.

### 3.5. Non existence conditions

From the analysis of the previous sections the unique solutions have a wave pattern consisting of three non overlapping waves in the following order: 1-wave, 2-Wave and 3-Wave have a unique solution. The only exception is when either of the following two conditions are satisfied

$$F_{L*} - F_L > 0, \quad F_L < -2$$

or

$$F_{L*} - F_R \leqslant 0, \quad F_R > 2$$

The first condition is compatible neither with 1-Wave rarefaction, see (46) nor with a 1-Wave shock due to energy considerations. The same reasoning is valid for the second condition, which is compatible neither with a 3-Wave rarefaction, see (51), nor with a 3-Wave shock due to the energy dissipation condition.

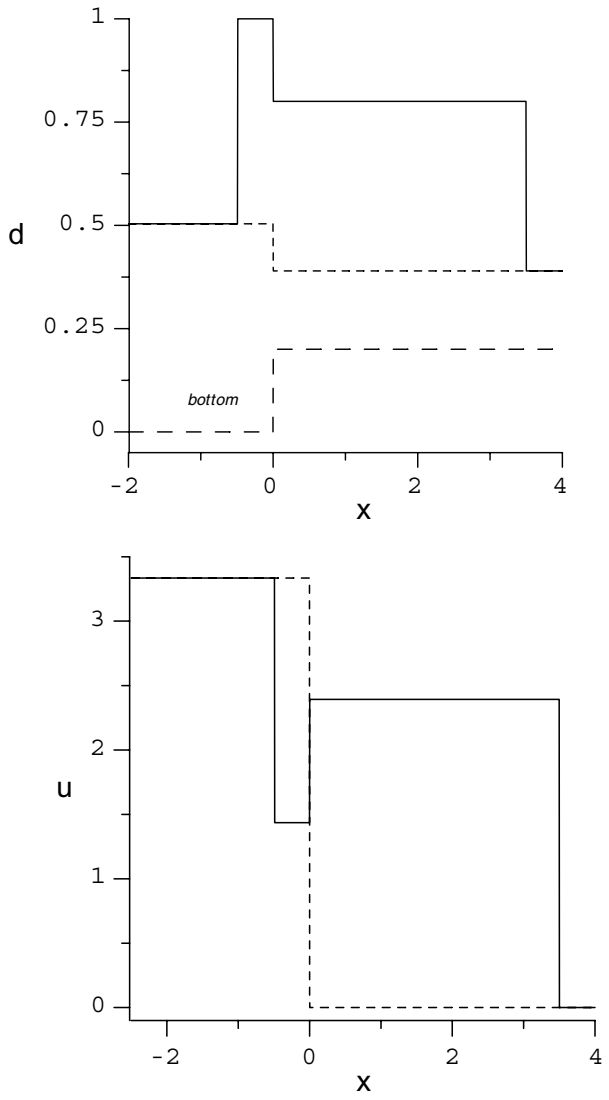


Fig. 15. Graph of the total depth and mean velocity for the supercritical motion case.

### 3.6. Solution algorithm

The solution of the problem is obtained by solving the derived non-linear system for internal states, either in the dimensional form (42) and (48) or in the non-dimensional form (45) and (50). In our numerical experiments the non dimensional form has been used throughout. Given a value for $\varepsilon$ the corresponding values of $\gamma_L$ and $\gamma_R$ can be determined and then the complete solution can be built. A sample flow chart of the procedure used to solve the local Riemann problem in the WAF numerical scheme can be found in Fig. 11

## 4. Examples

In this section we present some examples of possible solutions of the Riemann problem for system (1). The results are presented in the form of plots of the total depth and mean velocity at time $t = 0$ and time $t = 1$s. Recalling the considerations of Section 3.4 the examples are chosen to represent the possible combinations of allowed wave patterns. We set the acceleration due to gravity equal to $g = 9.81$. In all cases the

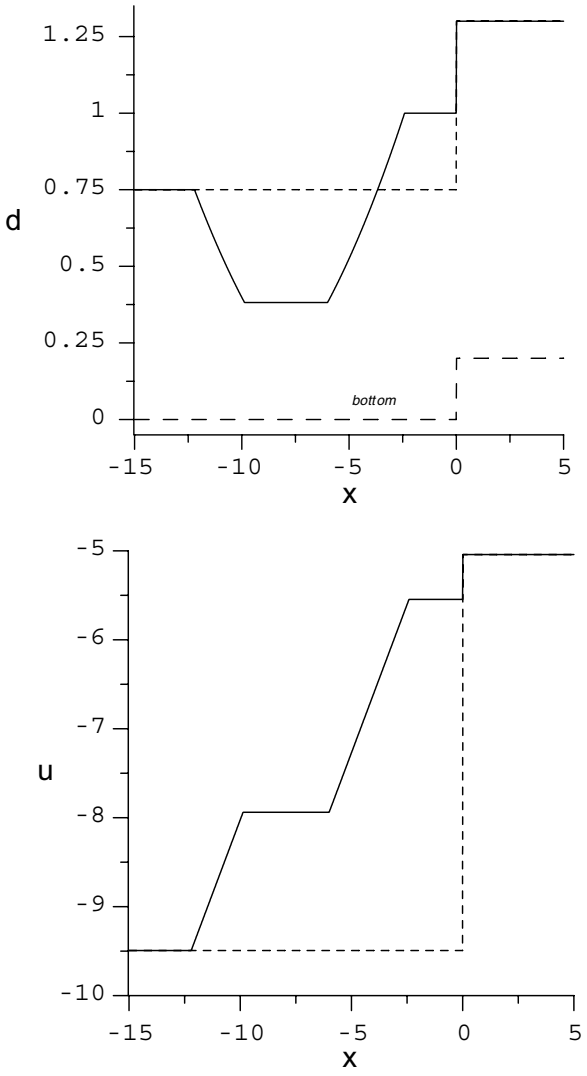


Fig. 16. Graph of the total depth and mean velocity for the negative supercritical motion case with two rarefaction waves.

bottom step is positioned at $x = 0$ and has the height of 0.2 to the right of the origin, see the dashed line on total depth plots.

### 4.1. Dam-break type problem

The dam-break case represents a combination of rarefaction and shock waves. The initial condition consists of two columns of water of different heights and is as follows:

$$d_L = 1.461837, \quad d_R = 0.308732, \quad F_L = F_R = 0.0$$

The solution is presented in Fig. 12 and contains a left moving rarefaction wave, a stationary shock at the step and a right-moving shock wave. The presence of the step leads to a reduction of the total water height running

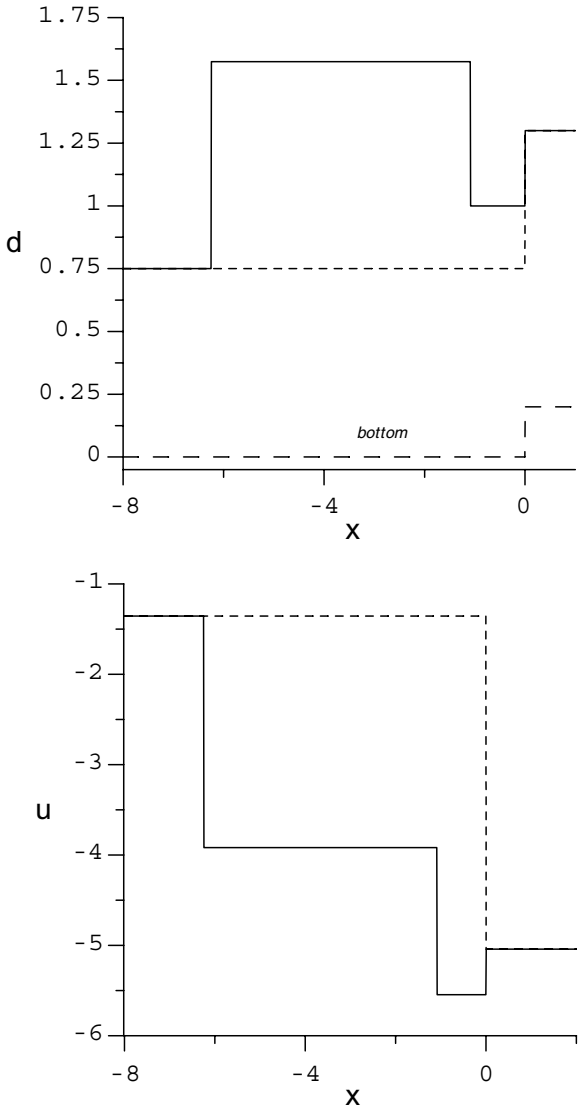


Fig. 17. Graph of the total depth and mean velocity for the negative supercritical motion case with two shock waves.

to the right as compared to the flat bottom case. This reduction is due to the stationary shock, which dissipates part of the energy of the shock wave.

### 4.2. Two rarefaction condition

In this case a divergent flow is simulated. The initial conditions are given by:

$$d_L = 2.597020, \quad F_L = -0.5$$
$$d_R = 4.62800, \quad F_R = 1.5$$

The solution is shown in Fig. 13. As expected, it contains two rarefaction waves moving away from the central stationary shock at the step. No significant difference is noted compared to the flat bottom solution due to the

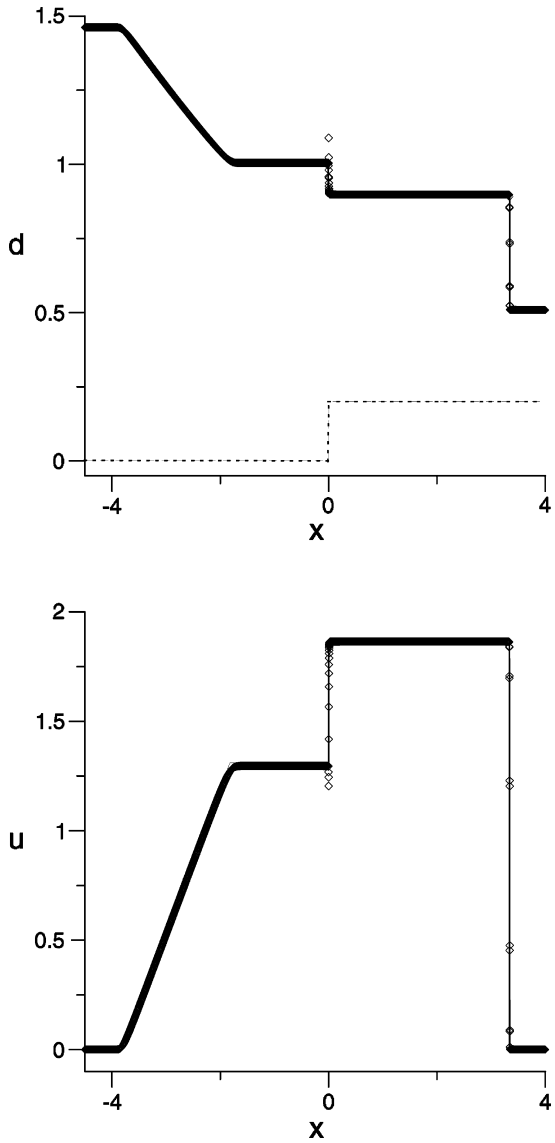


Fig. 18. Lax–Friedrichs (symbols) versus exact (solid line) solutions of Problem 4.1. A mesh of 10,000 cells is used in the numerical solution.

fact that the initial conditions do not induce any interaction between the travelling waves. Here the step has only a dissipative effect.

### 4.3. Two shock case

In this case a convergent flow is studied. The following initial conditions are used:

$$d_L = 0.568999, \quad F_L = 0.9$$
$$d_R = 0.568999, \quad F_R = 0.0$$

The solution is presented in Fig. 14. In this case the wave pattern is not different from that occurring in the case of flat bottom. As was noted in the previous example, the step acts as an energy dissipation mechanism.

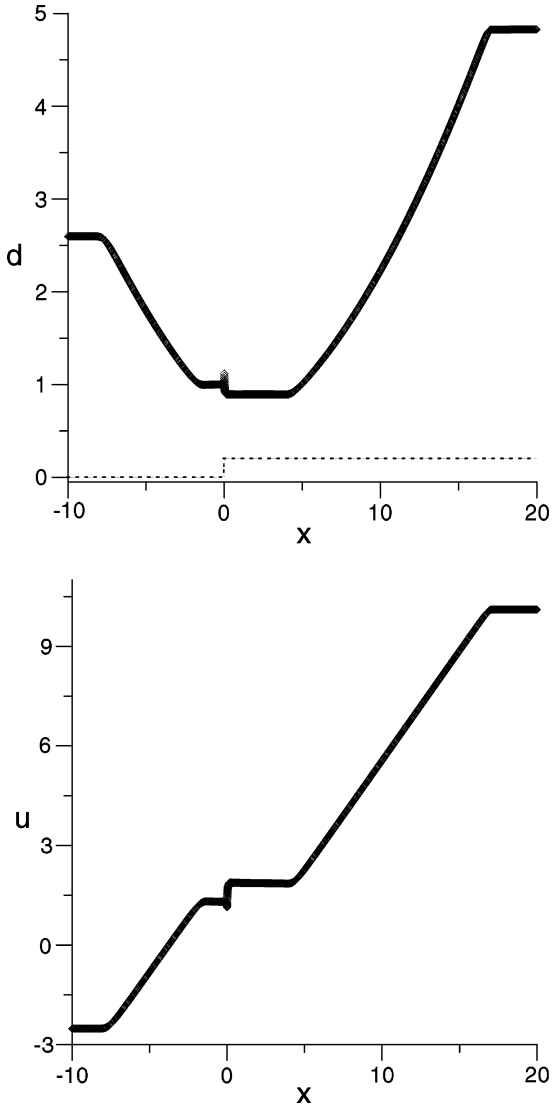


Fig. 19. Lax–Friedrichs (symbols) versus exact (solid line) solutions of Problem 4.2. A mesh of 10,000 cells is used in the numerical solution.

### 4.4. Supercritical condition

In this case a supercritical motion ($F_L > 1$) from the left is considered. The initial conditions are given by

$$d_L = 0.50370, \quad F_L = 1.5$$
$$d_R = 0.189824, \quad F_R = 0.0$$

The solution is presented in Fig. 15. In this case there is a clear difference in the wave pattern with respect to the flat bottom case: the presence of the step leads to the appearance of a left-moving shock wave. This is a way in which the signal coming from the left is reflected by the step even if its Froude number suggests that no signal can travel upstream. This could be due to a micro-mechanism by which a wave approaching the shore is reflected and refracted in a numerical scheme that uses the present exact solution of the Riemann problem.

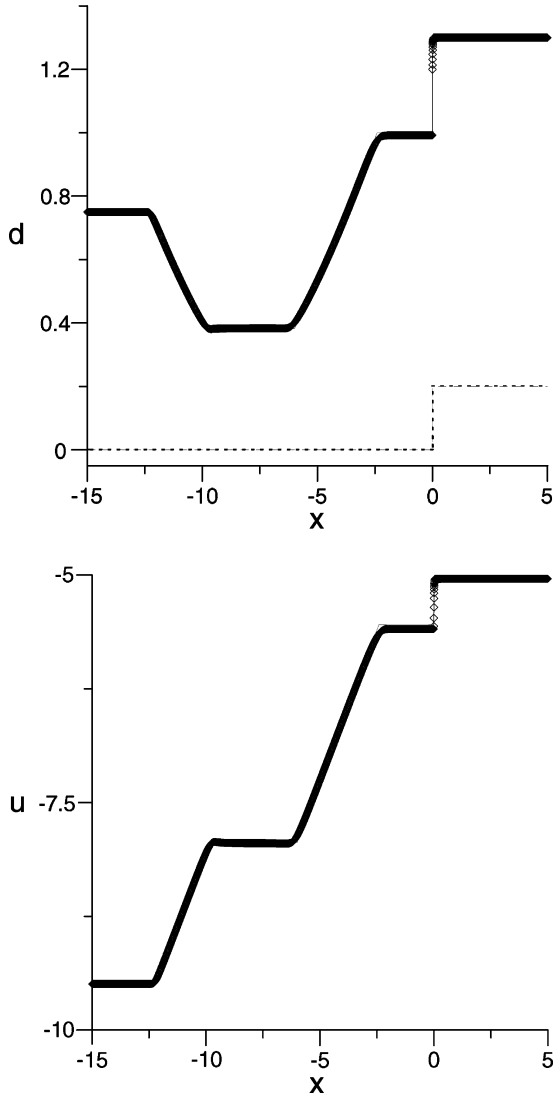


Fig. 20. Lax–Friedrichs (symbols) versus exact (solid line) solutions of Problem 4.5. A mesh of 10,000 cells is used in the numerical solution.

### 4.5. Negative supercritical motion

In this case a supercritical motion from right to left is considered. The initial conditions are given by:

$$d_L = 0.75, \quad F_L = -3.5$$
$$d_R = 1.1, \quad F_R = -1.5$$

The solution is presented in Fig. 16. This is the other extreme case where the solution differs significantly from the flat-bottom solution. The presence of the step introduces no limitation in the signal propagation downstream, and its effect is in dissipating energy by the stationary shock at the step. The other two waves propagate without any constraints. If the left Froude number is reduced a two shock case is obtained. The corresponding initial conditions are given by

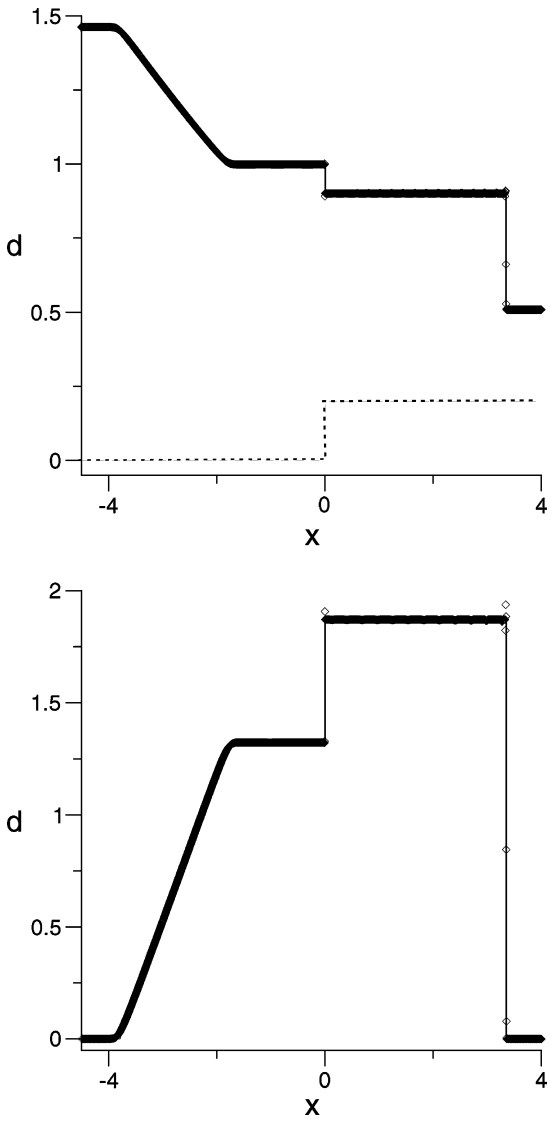


Fig. 21. Numerical solution by the WAF method on the mesh of 2000 cells (symbols) versus the exact solution (solid line) for Problem 4.1.

$$d_L = 0.75, \quad F_L = -0.5$$
$$d_R = 1.1, \quad F_R = -1.5$$

and the solution is shown in Fig. 17.

## 5. Comparison with numerical solutions

Here we show some comparisons of between the exact and numerical solutions. First we present an independent verification of the fact that our exact solution to the Riemann problem is correct, noting that we have introduced criteria to select a unique exact solution. We compare some of the exact solutions from the previous section with the numerical results of the first-order (very dissipative) Lax–Friedrichs scheme combined with a simple centred approximation for the source term.

Figs. 18–20 show the results of the numerical computations for a mesh of 10,000 cells for three different solution patterns. We observe that overall the numerical solution agrees very well with our exact solution. In particular, positions and types of all waves coincide. We note the (spurious) overshoots in the numerical solution near the step position.

We next show some preliminary results of the practical application of present Riemann solver in the framework of Godunov-type upwind methods. Here we use it in the WAF method [16–18,4,3], which is a second-order TVD schemes. A detailed explanation of the implementation of the Riemann solver in the framework of this method will be reported elsewhere. Fig. 21 shows the preliminary results of the WAF method on a coarse mesh of 2000 cells. We again observe good overall agreement between the numerical and exact solutions. The obvious improvement over the Lax–Friedrichs method is the absence of overshoots in the total depth profile at the step position and a better resolution of all waves.

## 6. Conclusions

The exact solution of the Riemann problem for the shallow water equations with a discontinuous step-like bottom geometry has been presented. The solution is built by first adding to the conventional system of the shallow water equations an additional equation for the bottom profile and then solving the new, extended system. Conditions for existence and uniqueness of the solution have been found. Using the conservation of mass and momentum, the Rankine–Hugoniot conditions for the stationary shock wave on the step have been derived. These conditions satisfy the principle of dissipation of energy. This together with an additional condition that a transition from subcritical to supercritical flow across the step is not allowed makes the solution unique.

Examples of solutions have been presented for some typical configurations. These illustrate some of the possible wave patterns which may occur in the Riemann problem solution. Next, the validity of the exact solution constructed here has been verified against a first-order dissipative finite-difference method, noting that good agreement is observed. Finally, we have used the proposed Riemann solver in a Godunov-type scheme for the shallow water equations with variable bottom geometry. Preliminary results look encouraging.

Future research will include the study of Riemann problems with vacuum in the initial data as well as a systematic development of Godunov-type methods using the proposed Riemann solver.

## Acknowledgments

The first author acknowledges the financial support provided by the University of Trento, Italy. The second author acknowledges the financial support provided by the PRIN programme (2004-2006) of the Italian Ministry of Education and Research (MIUR). The third author acknowledges the support of an EPSRC grant, as senior visiting fellow (Grant GR N09276) at the Isaac Newton Institute for Mathematical Sciences, University of Cambridge, UK, 2003.

## References

[1] F. Alcrudo, F. Benkhaldom, Solution to the Riemann problem of the shallow water equation with a bottom step, Comput. Fluids 30 (2001) 643–671.
[2] C.M. Bender, S.A. Orszag, Advanced Mathematical Methods for Scientists and Engineers, McGraw, 1978.
[3] M. Brocchini, A. Mancinelli, L. Soldini, R. Bernetti, Structure-generated macrovortices and their evolution in very shallow depths, in: Proceedings of the 28th I.C.C.E., vol. 1, Cardiff, UK, 2002, pp. 772–783.
[4] M. Brocchini, R. Bernetti, A. Mancinelli, G. Albertini, An efficient solver for near shore flows based on the waf method, Costal Eng. (2001).
[5] V.I. Bukreev, A.V. Gusev, V.V. Ostapenko, Breakdown of a discontinuity of the free fluid surface over a bottom step in a channel, Fluid Dyn. 38 (2) (2003) 889–899.
[6] T. Gallouet, J.-M. Herard, N. Seguin, Some approximate Godunov schemes to compute shallow-water equations with topography, Comput. Fluids 32 (4) (2003) 479–513.
[7] P. Glaister, Approximate Riemann solutions for the shallow water equations, J. Hydraulic Res. 23 (3) (1988) 293–306.
[8] S.K. Godunov, A finite difference method for the computation of discontinuous solutions of the equations of fluid dynamics, Mat. Sbornik 47 (1959) 357–393.
[9] J.M. Greenberg, A.Y. Leroux, R. Baraille, A. Noussair, Analysis and approximation of conservation laws with source terms, SIAM J. Numer. Anal. 34 (5) (1997) 1980–2007.
[10] K. Hu, C.G. Mingham, D.M. Causon, Numerical simulation of wave overtopping of coastal structures using the non-linear shallow water equations, Coastal Eng. 41 (4) (2000) 433–465.
[11] P.G. LeFloch, Mai Duc Thanh, The Riemann problem for fluid flows in a nozzle with discontinuous cross-section, Preprint NI03024-NPA, Isaac Newton Institute for Mathematical Sciences, University of Cambridge, UK, 2003.
[12] R.J. LeVeque, Balancing source terms and flux gradients in high-resolution Godunov methods: the quasi-steady wave-propagation algorithm, J. Comput. Phys. 146 (1998) 346–365.
[13] J. Lighthill, Waves in Fluids, Cambridge University Press, 1978.
[14] P.L. Roe, Upwind differencing schemes for hyperbolic conservation laws with source terms, in: Carasso, Raviart, Serre (Eds.), Proceedings of the First International Conference on Hyperbolic Problems, Springer, 1986, pp. 41–51.
[15] J.J. Stoker, Water Waves, Interscience, New York, 1957.
[16] E.F. Toro, A weighted average flux method for hyperbolic conservation laws, Proc. Roy. Soc. London A423 (1989) 401–418.
[17] E.F. Toro, Riemann problems and the WAF method for solving two-dimensional shallow water equations, Phil. Trans. Roy. Soc. London (1989) 43–68.
[18] E.F. Toro, Shock-Capturing Methods for Free-Surface Shallow Flows, Wiley and Sons Ltd., 2001.
[19] M.E. Vazquez-Cendon, Improved treatment of source terms in upwind schemes for the shallow water equations in channels with irregular geometry, J. Comput. Phys. 148 (1999) 497–526.